This is a preprint, the final version is subject to change, of the American Mineralogist (MSA)
Cite as Authors (Year) Title. American Mineralogist, in press.
DOI: https://doi.org/10.2138/am-2019-6852CCBY

REVISION 1

The condensation temperatures of the elements: a reappraisal

Bernard J. Wood

Duane Smythe

Thomas Harrison

University of Oxford

Department of Earth Sciences

South Parks Road

Oxford OX1 3AN

U.K.

Abstract

As part of a project to investigate the volatilities of so-called "moderately volatile elements" such as Zn, In, Tl, Ga, Ag, Sb, Pb and Cl during planetary formation, we began by re-calculating the condensation temperatures of these elements from a solar gas at 10^{-4} bar. Our calculations highlighted three areas where currently available estimates of condensation temperature could be improved. One of these is the nature of mixing behavior of many

important trace elements when dissolved in major condensates such as silicates, Fe-rich metals and sulfides. Nonideal solution of the trace elements can alter (generally lower) condensation temperatures by up to 500 K. Secondly, recent measurements of the halogen contents of CI chondrites (Clay et al. 2017) indicate that the solar system abundance of chlorine is significantly overestimated and this affects the stabilities of gaseous complexes of many elements of interest. Finally, we have attempted to improve on previous estimates of the free energies of chlorine-bearing solids since the temperature of chlorine condensation has an important control on the condensation temperatures of many trace elements. Our result for the 50% condensation temperature of chlorine, 472 K is nearly 500 K lower than the result of Lodders (2003) and this means that the HCl content of the solar gas at temperatures < 900 K is higher than previously estimated.

We based our calculations on the program PHEQ (Wood and Hashimoto 1993) which we modified to perform condensation calculations for the elements H, O, C, S, Na, Ca, Mg, Al, Si, Fe, F, Cl, P, N, Ni and K by free energy minimisation. Condensation calculations for minor elements were then performed using the output from PHEQ in conjunction with relevant thermodynamic data. We made explicit provision for nonidealities using information from phase diagrams, heat of solution measurements, partitioning data and by using the lattice strain model for FeS and ionic solids and the Miedema model for solutions in solid Fe. We computed the relative stabilities of gaseous chloride, sulfide and hydroxide species of the trace elements of interest and used these, as appropriate in our condensation calculations. In general, our new 50% condensation temperatures are similar to or, because of the modifications noted above, lower than those of Lodders (2003).

1. Introduction

The concept of volatility is an important one in geochemistry and cosmochemistry. During the early evolution of the solar system there was fractionation of volatile elements between solid, gas and liquid phases, resulting in the isotopic and chemical fractionations observed between different meteorite groups and planetary bodies. One of the principal tasks in this area is to determine how to interpret the observed chemical and isotopic differences between different bodies in terms of appropriate processes in the solar nebula and during planetary accretion. In this context it is necessary to consider exactly what is meant by "volatility". Conventionally, volatility is defined geochemically in a very broad sense as being related to the temperature at which a specific element would condense from a gas of solar composition. Thus, volatile elements are defined as those which condense at relatively low temperature (e.g. < 1100 K) from the putative solar gas while refractory, involatile elements condense at higher temperatures. The utility of the approach lies in the fact that elemental abundances in the bulk silicate Earth (BSE) correlate negatively with condensation temperature when expressed relative to a volatile-rich meteorite group such as CI chondrites.

Figure 1 shows the abundances of a large number of elements in the BSE, expressed relative to abundances in CI chondrites, (and normalised to Mg of 1.0) (Palme and O'Neill 2014) plotted versus the temperature (Lodders 2003) at which 50% of the element would be condensed from a gas of solar composition at a total pressure of 10^{-4} bar. As can be seen, *refractory* lithophile elements such as Ca, Ti, Zr, Sc and the rare earths (REE) are all present in approximately chondritic proportions one to another in the silicate Earth, while there is a steady decline in abundance of lithophile elements with decreasing condensation temperature beginning at Mg. The latter has a 50% condensation temperature (T_{50}) of 1336 K (Lodders 2003). Lying below the volatility "trend" of lithophile elements are the abundances of

siderophile elements which are known to have strong affinities for liquid Fe and are hence believed to be partly partitioned into the core. The so-called highly siderophile elements, encompassing the platinum group, Au and Re are present in approximately chondritic ratio one to another in the BSE, but at <1% of the level of refractory lithophiles. On the left side of Figure 1 we have grouped together elements which are depleted relative to elements of similar volatility (or condensation temperature) and arbitrarily named them "volatile siderophile" elements. Some of the latter, Sb, Ag, S, and C for example are well-known to partition strongly into Fe-rich metals (Pei et al. 1995; Steelmaking Data Sourcebook1988; Wood 1993) while others (e.g. Cl) are depleted but not known to partition into liquid Fe so the reasons for their low abundances are unclear. Note, however, that a recent re-analysis of CI chondrites (Clay et al. 2017) raises the CI normalised concentration of chlorine by a factor of 6.1.

The correlation shown in Figure 1 for lithophile elements is seductive, but liable to draw the reader into overinterpretation of geochemical and cosmochemical data because abundances correlate with a process, condensation, which applied only for a brief period in the history of the solar system. The nebular gas of approximately solar composition appears to dissipate within about 3 Ma of the beginning of the solar system (Evans et al. 2009) so that most of the 10s of millions of years of planetary growth and even the geological development of small asteroidal bodies such as Vesta (Roszjar et al. 2016) took place in the absence of the H_2-rich atmosphere characteristic of the bulk solar system. The nebular gas is, of course, highly reducing (about 7 log fO_2 units below the Fe-FeO, IW oxygen buffer) and after it disappeared the atmospheres above protoplanetary bodies would have been established by silicate-gas equilibria under oxygen fugacity conditions governed by the FeO contents of the silicate mantle. If we take the lowest fO_2 values plausible, then these would have been controlled, given the presence of metallic cores on the terrestrial planets and many asteroids,

by Fe-FeO equilibrium and would thus have been 1-2.5 log units below IW (Righter et al. 1998; Wood et al. 2006).

Despite these observations on the short lifetime of the nebular gas and the inevitable increase in fO_2 after it disappeared, the condensation sequence shown in Figure 1 appears to have taken on near-magical significance in the literature. Thus, for example, the difference in abundances of Zn and S in the silicate Earth has been used to infer that the S "missing" from silicate Earth is partitioned into the core and that the difference in Zn/S between CI chondrites and BSE can be used to calculate the S content of the core (Dreibus and Palme 1996). The result is 1.7 % S (Dreibus and Palme 1996). The large difference in relative abundance between In and elements of similar volatility such as Tl is often treated as an unexplained anomaly (Witt-Eickschen et al. 2009) an impression enhanced by the fact that In is both more siderophile and more chalcophile than the more depleted Tl (Kiseeva and Wood 2013; Wood et al. 2014). However, In (+3) and Tl (+1) have different oxidation states in many geologic environments so their relative volatilities must depend on oxygen fugacity, with indium becoming, in principle less volatile as fO_2 increases. This assertion follows from the idealised equilibrium:

$$2In^0\,(gas) + Tl_2O\,(solid) + O_2 = 2Tl^0\,(gas) + In_2O_3\,(solid) \quad (1)$$

Raising fO_2 should, in this case drive the equilibrium to the right, putting Tl into the gas phase and In into the solid.

Our study started from the question "Are the calculated condensation temperatures from a solar gas relevant to elemental abundances in silicate Earth?". We began by performing condensation calculations for 30 of the more volatile elements. These convinced us that the results are very sensitive to the wide range of possible assumptions for the properties of the trace elements dissolved in the major phases. For example, we are able to

reproduce the result of Lodders (2003) for Ag and Pb dissolved in solid Fe assuming ideal solution, but when we take account of the likely nonidealities of Ag and Pb in Fe, the condensation temperatures drop by several hundred K. As we progressed through most of the naturally occurring elements we found that the behavior of Cl in the solar gas has major influences on the properties of many of the elements and that the recently re-determined halogen contents of the solar system (as in CI chondrites, Clay et al. 2017) should change condensation temperatures significantly. We therefore determined to revise the published values to take account of the new measurements.

2. Calculation Strategy: Condensation from a solar gas

Many of the calculations discussed below can and were performed in a spreadsheet. The first step, however, is to determine the stabilities of the solids and gaseous species of the major elements. To do this we used the computer program PHEQ (Wood and Hashimoto 1993) which performs free energy minimisation for fixed total gas pressure and temperature and provides the number of moles of each species for a known starting composition. It was written specifically for performing condensation calculations and, as initially configured, uses free energy data for 93 gaseous and 148 solid species of the elements H, O, C, S, Na, Ca, Mg, Al, Si, and Fe. These are tabulated in 100 K intervals the form:

$$\frac{\mu^0}{RT} = \frac{H_T^0 - H_{298}^0 - TS_T^0 + \Delta H_{f,298}^0}{RT} \qquad (2)$$

In equation (2) H^0 and S^0 refer to enthalpy and entropy of the pure phase at the subscripted temperature and $\Delta H_{f,298}^0$ to the enthalpy of formation from the elements at 298 K. For reasons which will become clear as we continue, we have added solid and gas data for species of the elements F, Cl, P, N, Ni and K. Other updates and modifications of PHEQ described in the literature include the GRAINS code of Petaev (2009). Although the PHEQ

program, as initially configured, assumes ideal solution for olivines, orthopyroxenes, clinopyroxenes, plagioclases, metals, spinels and melilite this assumption introduces only small errors in T_{50} for the major elements Na, Ca, Mg, Al, Si and Fe which, except for Na, all condense above 1300 K. The calculated condensation temperatures for these elements agree well with those of Lodders (2003) and of earlier workers on this subject (Table 2). Most of the minor elements of interest condense into Fe metal or iron sulphide, however, and we have made explicit provision for nonideal solution in these cases as detailed below.

Calculations were performed at a total pressure of 10^{-4} bar and we followed normal convention of re-equilibrating solids and gases at each step in the condensation process as temperature declined. Although there are a number of estimates of solar system abundances of the elements, we opted, apart from the halogens, to use those of Lodders (2003) in order to facilitate comparison with her calculations of condensation temperature.

Figure 2 shows the abundances of the important solid phases and gas components as functions of temperature at 10^{-4} bar. Small amounts of corundum appear at about 1675 K, followed by hibonite at 1630 K, melilite at 1550 K and spinel at 1410 K. Major forsteritic olivine and Fe-rich metal start precipitating at 1380-1360 K, followed by other silicates, clinopyroxene, plagioclase and orthopyroxene at 1350, 1305 and 1285 K respectively. With declining temperature the proportions of these phases change as they react with one another and with the solar gas. The other major phase to appear is iron sulfide at 710 K and this increases in proportion at the expense of Fe metal as temperature falls further (Fig. 2). Table 1 gives the major solid and gaseous species in 50^{o} intervals from 1700 down to 350 K together with the fugacities of H_2O, O_2, HCl and H_2S at each temperature. We reiterate that these are **equilibrium** calculations, however and that it has been shown that some of the

expected reactions, notably the reduction of N_2 and CO to NH_3 and CH_4 are kinetically inhibited at low temperatures (Lewis and Prinn 1980).

2.1 Trace and Minor element condensation

Our general approach to condensation can be carried out for most elements in a spreadsheet. Let us suppose that our trace element M is present in the gas phase predominantly as monatomic M^0 and that it condenses to oxide $MO_{1.5}$. The condensation equilibrium can be represented as follows:

$$M^0(\text{gas}) + 0.75\ O_2\ (\text{gas}) = MO_{1.5}\ (\text{solid}) \qquad (3)$$

The logarithm of the equilibrium constant for the reaction ($\log K_r$) is calculated from the tabulated equilibrium constants of formation of the species involved from their constituent elements:

$$\log K_r = \log K_f^{MO_{1.5}} - \log K_f^{M^0} - 0.75 \log K_f^{O_2} \qquad (4)$$

We fit $\log K_r$ as a function of temperature or reciprocal temperature. Then, from the equilibrium constant for reaction (3) we have:

$$\log p_{M^0} = \log a_{MO_{1.5}}^{\text{solid}} - \log K_r - 0.75 \log p_{O_2} \qquad (5)$$

Where p_{M^0} and p_{O_2} are the partial pressures of M^0 and O_2 in the gas phase, respectively, and $a_{MO_{1.5}}$ is the activity of the metal oxide in the condensing solid. We obtain $\log p_{O_2}$ as a function of temperature from the PHEQ program and as a starting point assume that $MO_{1.5}$ is a pure oxide with $a_{MO_{1.5}}$ equal to 1. We fix p_{M^0} at the value expected at a total gas pressure of 10^{-4} bar when 50% of the solar abundance of M is in the gas phase. We then vary temperature until the left- and right-hand sides of Equation (5) are equal. This gives us T_{50}.

Exactly the same approach is used if, for example, the most stable gaseous species is MCl or MS or MOH. In these cases, however, the equilibrium must also use appropriate log K and partial pressure data for HCl, H_2S, H_2O and H_2. If two or more gaseous species are present in similar amounts, we simply reduce log p_i for the most stable species by an appropriate amount to take account of the fractions of these additional species.

The simplified case above describes condensation into a pure solid phase of element M to $MO_{1.5}$. Higher condensation temperatures are obtained, however, if we consider the fact that trace elements will, in general, dissolve in one or more of the major phases described above and illustrated in Figure 2. This is because the activity of any component *i* (a_i) is generally lowered relative to that of pure *i* ($a_i = 1$) if *i* is dissolved in a major element phase P:

$$\log a_i = n \log (X_i)_\mathrm{P} + n\log \left(\gamma_i\right)_\mathrm{P} \qquad (6)$$

In Equation (6) *n* refers to the number of sites in phase P on which *i* substitutes, X_i is the mole fraction of *i* on those sites, and $(\gamma_i)_P$ is the activity coefficient of *i* in phase P. Mole fraction X_i comes from having 50% of element *i* in the solid phase. If the solid solution is ideal $(\gamma_i)_P$ is 1.0 and *i* will condense into P so long as the sum of the second and third terms on the right hand side is less than zero i.e.

IF: $\log (X_i)_P + \log (\gamma_i)_P < 0$, condensation of *i* is into phase P

ELSE: *i* condenses into pure *i* at lower temperature

In order to calculate activities and condensation temperatures in cases of dissolution in a major phase, we started with the phases nominated by Lodders (2003) as the hosts and searched for other solutions in cases where it seemed likely that such existed.

2.2 Activity Coefficients of trace elements

We used a combination of phase equilibria, thermodynamic data and crystallographic measurements to make estimates of the activity coefficients of trace elements in the major solid phases in the condensation sequence.

2.2.1 Activity coefficients in solid Fe from solubility. At temperatures below 1185 K, the stable form of Fe is body-centred-cubic α-Fe while face-centred cubic γ-Fe is stable between 1185 and 1667 K. For elements such as Ag and Pb which are almost insoluble in solid Fe we estimate activity coefficients from known solubility at fixed temperature. Thus, for example, in equilibrium with pure Ag the maximum mole fraction of Ag dissolved in γ-Fe at 1366 K is $3.7\text{x}10^{-5}$ (Wriedt et al. 1973). A first estimate of the activity coefficient at this temperature would then be:

$$\gamma_{\mathrm{Ag}} = 1/X_{\mathrm{Ag}} = 1/(3.7\text{x}10^{-5}) = 27027$$

At this temperature the Ag is liquid, however so we should make a correction for the free energy of the liquid-solid transformation in pure Ag. This makes γ_{Ag} larger by a factor $f_{s\text{-}l}$:

$$\mathrm{f_{s-l}} = \exp\left(\Delta S_{\mathrm{fus}}\left(T - T_{fus}\right)/(\mathrm{R}T)\right) \qquad (7)$$

where ΔS_{fus} is the entropy of melting at the melting temperature of 1234 K, T is the temperature of interest and R is the gas constant.

In order to extrapolate a known (or estimated) value of γ_i up and down temperature we make the usual assumption that activity coefficients approach 1 at infinite temperature. This leads to a calculated γ_T at temperature T, from $\gamma_{T_{\mathrm{M}}}$ measured at temperature T_{M}:

$$\ln(\gamma_T) = (T_{\mathrm{M}}/T) \cdot \ln(\gamma_{T_{\mathrm{M}}}) \qquad (8)$$

2.2.2 Activity coefficients in Fe from Miedema model. Where the Fe – M (M being the minor element of interest) phase diagram is complex such that extraction of activity coefficients is difficult, we have used the semi-empirical Miedema model (Boom et al. 1983; Miedema et al. 1980) to estimate activity coefficients in the solid Fe alloy. This model for the energetics of mixing of binary alloys has 3 parameters for each element, an electron density parameter, the work function of the metal and the atomic surface area. It has been found to successfully predict alloying behavior in a large number of cases. We did not re-calculate heats of mixing using the Miedema model but have simply adopted published values calculated for binary alloys with Fe (Boom et al. 1983).

2.2.3 Activity coefficients from lattice strain theory. Insertion of a 'foreign' ion into a crystal lattice generally requires that the lattice relaxes to accommodate the ion which will, in general, have different radius and sometimes charge from those of the major ion which it is replacing. Thus, for example, in the case of chalcophile elements such as Pb, Cd or Zn dissolving in FeS, the differences in ionic radius between Fe and the substituent trace element leads to a positive free energy of strain around the cation defect. If we treat the lattice as elastically isotropic, the strain free energy per mole of substituent can be shown to be (Blundy and Wood 1994; Brice 1975):

$$\Delta G_{\text{strain}}^{\text{crystal}} = 4\pi \mathrm{E_S N_A}\left(\frac{\mathrm{r_\circ}}{2}(r_\circ - r_i)^2 - \frac{1}{3}(r_\circ - r_i)^3\right) \qquad (9)$$

In Equation (8), E_S is the Young's modulus of the site, N_A is Avogadro's Number, r_i is the radius of the substituent (Pb, Cd or Zn in this case) and r_o is the radius of the cation which fits without strain into the lattice. In the case of FeS, r_o is assumed to be the ionic radius of Fe^{2+}. In cases where the Young's modulus is unknown we use the bulk modulus for the crystal K and convert assuming a Poisson's ratio of 0.25 yielding E = 1.5K (Blundy and Wood 1994).

250 The strain free energy leads to an activity coefficient of:

251 $$\gamma_i = \exp \frac{\Delta G_{\text{strain}}^{\text{crystal}}}{\text{R}T} \qquad (10)$$

252 We used this approach for substitution of elements into phases (other than Fe) for which no
253 thermodynamic, partitioning or solubility data were available.

254 **2.2.4 Activity coefficients from thermodynamic or partitioning data.** In some cases there
255 have been direct measurements of the thermodynamic properties of the minor elements of
256 interest and these yield estimates of the activity coefficients. There are, for example,
257 measurements of the enthalpies of mixing of the systems Fe–Ga and Fe–Ge (Predel and
258 Vogelbein 1975, 1979) and these can be turned into partial molar enthalpies of solution of Ge
259 and Ga in solid Fe. These partial molar enthalpies H_s are then converted into activity
260 coefficients using an analog of Equation (10)

261 $$\gamma_i = \exp \frac{H_s}{\text{R}T} \qquad (11)$$

262 A final method of estimating γ_i is from partitioning between liquid and crystals. In
263 this case we assume that the ratio of crystal–liquid partition coefficients D_i and D_o for the
264 trace ion of interest (i) and the major ion of the host crystal (o) can be inverted to give
265 activity coefficient (Davis et al. 2018) i.e.

266 $$\frac{D_i}{D_o} \sim \frac{1}{\gamma_i} \qquad (12)$$

267 **3. High Temperature condensation (> 1300 K) of metals and oxides**

268 **3.1 Elements forming simple alloys or metals: Os, Ir, Ru, W, Re, Mo**

At high temperatures (> 1300 K) in a solar gas, the dominant species of many elements is the uncharged atom M^0. This makes calculation of condensation temperature into one of the stable phases of Figure 2 relatively straightforward or, even easier in the cases of elements which condense at higher temperatures into pure metal or oxide. Os is calculated to condense to Os metal at 1806 K. Ir would be expected to form a solid solution with Os and we assumed it dissolves ideally in Os-Ir alloy, giving a T_{50} of 1566 K. Ru should also alloy with osmiridium and making this assumption yields T_{50} of 1533 K for Ru.

The dominant gas species of W is calculated to be WO and W is calculated to form an alloy with Re with T_{50} of 1736 K for both elements. Similarly, Mo metal should form at high temperature with T_{50} of 1520 K.

3.2 Elements condensing into Fe metal

As soon as metallic Fe appears (1380 K) Rh, Pt, Pd, and V which have very low activity coefficients (<<1) in Fe, begin to dissolve in it. We used the Miedema model for activity coefficients (Boom et al. 1983) and calculated T_{50} values of 1370, 1370, 1330 and 1370 K for these four elements. Ni also dissolves into Fe with a T_{50} value of 1363 K followed by Co at 1354 and Cr (1291) all condensing from M^0 in the gas to the Fe-rich metal with small nonidealities (Table 2).

For phosphorus we followed Lodders (2003) and assumed that $(Fe,Ni)_3P$ is a potentially stable phase. The most stable gas species at high temperatures are P_2, PO and PS. We used experimental data on P_2 partial pressures above phosphides (Zaitsev et al. 1995) to calculate the thermodynamic properties of Fe_3P which were added to the PHEQ database. The properties of Ni_3P were taken from Barin (1989). $(Fe,Ni)_3P$ was found to appear at 1310 K with a T_{50} of 1287K for phosphorus.

3.3 Refractory lithophiles: Y, Sc, Ti, Nb, Ta, U, Th, Zr, Hf and the lanthanides

Most of these elements are so oxyphile that the most stable gas species, even in the reducing solar gas is MO or MO_2 rather than M^0. Ti is calculated to condense from TiO in the gas into $CaTiO_3$ perovskite, starting at 1583 K with a T_{50} of 1565 K. Many of these refractory lithophiles are very compatible in perovskite (Corgne and Wood 2005) and will, depending on their properties, condense into it (below 1583 K) or into hibonite (at temperatures below its appearance at 1630 K). The lanthanides are also very compatible in gehlenite-rich melilite (Nagasawa et al. 1980) so we can assume that this also becomes a host for the REE at temperatures below its appearance at 1550 K. For the lanthanides we used thermodynamic data on the gaseous oxides (Konings et al. 2014) and the gaseous element (Barin et al. 1989) to compute the stable gas species and the temperature of condensation of the oxide, which was assumed to dissolve in hibonite, perovskite and/or melilite as discussed above. For the elements Sm, Eu, Tm and Yb the most stable gaseous species is M^0. For all the other REE except Ce it is MO while for Ce it is CeO_2. A number of elements are calculated to dissolve in hibonite almost as soon as it appears at 1630 K (La, Nd, Gd, Tb, Dy, Ho, Er, Tm, and Lu). This is largely because their mole fractions are so low relative to Ca in the gas phase that their activities, taking account of the activity coefficients of Davis et al. (2018) (Eq. 6) in the solid are $<10^{-4}$. Three lanthanides Sm, Pr, and Yb dissolve in hibonite together with perovskite and melilite at slightly lower temperatures. The two elements which are not M^{3+}, Eu^{2+} and Ce^{4+} should condense primarily into melilite and perovskite at 1491 and 1454 K, respectively. For yttrium we used data on the properties of YO gas (Pedley and Marshall 1983) to calculate condensation into melilite, hibonite and perovskite with T_{50} of 1551 K. The stable ScO gas species is calculated to similarly condense into melilite and perovskite with T_{50} of 1541 K.

316 In a solar gas, the dominant Zr species at high temperatures are ZrO and ZrO_2 and
317 these condense to form solid ZrO_2 with T_{50} of 1722 K. For Hf we obtained the
318 thermodynamic properties of HfO (gas) from Pedley and Marshall (1983) and calculated
319 condensation to the pure HfO_2 solid (Barin et al. 1989) at 1720 K (T_{50}). Assuming ZrO_2 and
320 HfO_2 form a solid solution has insignificant effect because the condensation temperatures are
321 virtually identical.

322 Ta has stable gas species of TaO and TaO_2 and 50% condensation as Ta_2O_5 is
323 calculated to occur at 1546 K if Ta dissolves ideally in perovskite. A value of 1561 K is
324 obtained for Nb condensing as NbO and NbO_2 into perovskite.

325 The most stable gaseous species of Th is ThO_2 in the solar gas. Assuming ideal
326 solution of Th in hibonite, perovskite and melilite we obtain T_{50} for Th of 1630 K with
327 hibonite as the principal host. For U we obtained the thermodynamic properties of the
328 gaseous oxides from Konings et al. (2014) and obtained a similar result to Th for
329 condensation into hibonite (T_{50} = 1609 K), given the properties of UO_2 (solid) from Barin et
330 al. (1989).

331 Ba and Sr are also refractory and potentially stabilised by solution in perovskite. We
332 used thermodynamic data for $BaTiO_3$ and $SrTiO_3$ (Barin et al. 1989) and used the elastic
333 strain model with r_o of 1.18 Å and E_S 130 GPa (Corgne and Wood 2005) to calculate activity
334 coefficients using the 8-coordinate ionic radii of Shannon (1976). This leads to T_{50} values of
335 1548 and 1423 K for Sr and Ba, respectively.

336 Finally, Be condensation was treated using the thermodynamic data for BeO (solid),
337 BeO (gas), and Be (gas) and, assuming condensation into melilite, T_{50} is 1550 K, essentially
338 at the point of melilite appearance.

This is a preprint, the final version is subject to change, of the American Mineralogist (MSA)
Cite as Authors (Year) Title. American Mineralogist, in press.
DOI: https://doi.org/10.2138/am-2019-6852CCBY

4. Condensation at temperatures < 1300 K

4.1 Condensation of Cl, F, Br, and I

Cl is cosmochemically abundant and forms stable gas species with many of the elements of interest, predominantly at temperatures below 1100 K. Figure 3 shows calculated MCl/M^0 ratios for a number of elements of interest as a function of temperature at 10^{-4} bar in the solar composition gas. Because of the stabilising effect of gaseous Cl (as HCl) on other gas species at low temperatures, the temperature of condensation of Cl into solid phases is critical to the calculation of condensation temperature for a number of the other elements of interest. If, for example, in the regime below 800 K Cl is uncondensed, then elements such as In are stabilised in the gas relative to the solid by the presence of gaseous chlorides.

Lodders (2003) notes that the condensation temperatures of the halogens are uncertain and gives T_{50} for F, Cl, Br and I of 734, 948, 546 and 535 K, respectively. The relatively abundant Cl was considered to condense into sodalite ($Na_4Al_3Si_3O_{12}Cl$), at 948 K, this phase occurring in some carbonaceous chondrites. Sodalite is also a stable phase at high temperatures in some alkaline silica-undersaturated rocks.

In order to derive thermodynamic data for sodalite we used calorimetric measurements of third law entropies, heat capacities and enthalpy of formation (Komada et al. 1995). We then tested these against the reversed phase equilibrium experiments of Sharp et al. (1989) who determined the equilibrium boundary for the breakdown of sodalite to β-nepheline plus sodium chloride:

$$Na_4Al_3Si_3O_{12}Cl = 3NaAlSiO_4 + NaCl \qquad (13)$$

Sodalite was determined to be the stable assemblage at pressures up to about 0.8 GPa in the temperature range 900-1100 K (Sharp et al. 1989). Using the equations of state of

Sharp et al. (1989) we used the phase equilibrium results to estimate that the free energy change of reaction (13) at 1 bar lies in the range 16.0 to 16.9 kJ at 923-1073 K. In order to reproduce these values and to generate the apparent change in P-T slope of the reaction from negative to positive above about 1000 K we followed Sharp et al. in adding entropy of Al-Si disorder in sodalite above 800 K. We find that adding 35 $J \cdot K^{-1}$ of additional entropy (Sharp et al. assumed 30.85 $J \cdot K^{-1}$) yields the observed free energies of reaction.

We added the free energy functions for sodalite, NaCl and KCl (both from Barin et al., 1989) to the PHEQ database and calculated the condensation sequence in the normal way. This leads to a condensation temperature (T_{50} of 410 K) with NaCl and KCl as the major solid Cl-bearing phases if we use the original, Lodders (2003) abundances of Cl. Sodalite appears at about 390 K and rapidly consumes NaCl at lower temperatures.

Paradoxically, the new, lower solar system abundances of Cl (Clay et al. 2017) lead to higher T_{50} values for Cl. This is because Cl begins to condense into fluorapatite soon after it appears at 675 K if the original high Cl abundances (Lodders 2003) are used. In this case about 1/3 of the Cl condenses as chlorapatite until all P is consumed, but T_{50} for Cl is not reached until NaCl and KCl start to precipitate at 410 K. When we revert to the new lower Cl abundances, more than 50% of the Cl condenses into fluorapatite-chlorapatite solutions before halides or sodalite become stable. This therefore increases T_{50} for Cl which becomes dependent on the thermodynamic properties of chlorapatite. To perform these calculations we added to the PHEQ database thermodynamic data for fluorapatite (Hovis and Harlov 2010; Robie et al. 1978), hydroxyapatite and chlorapatite (Drouet 2015) together with the properties of a large number of gaseous species from Barin et al. 1989, detailed in Supplementary Table 1, combined with those of PH, PN, PH_3 (Lodders 1999) and PS (Lodders 2004). P begins to condense into $(Fe,Ni)_3P$ at 1310 K (discussed above) but this phosphide starts being consumed when fluorapatite appears (675 K) and is completely lost at 590 K. The enthalpy of

formation of chlorapatite, $Ca_5(PO_4)_3Cl$, has been measured a number of times, with a spread from -6639 to -6548 kJ (Drouet 2015) which produces considerable uncertainty in the condensation temperature of this component of apatite. Hovis and Harlov (2010) also determined large apparent nonidealities in fluor-chlorapatite solid solutions, which, if applied at face value would substantially lower the condensation temperature of Cl. These authors suggested, however that their calorimetric measurements were influenced by anion vacancy defects in their synthetic apatite crystals and that the fluorapatite-chlorapatite series is essentially ideal. We commenced with an enthalpy of formation (-6580.35 kJ) in the middle of the measured range and assumed ideal solution. In this case chlorapatite appears in solid solution in fluorapatite (which itself condenses rapidly at 675 K) at about 610 K. The chlorapatite component then condenses over an extended temperature interval with T_{50} of 472 K. Lowering the enthalpy of formation to that determined by Cruz et al. (2005) (-6615.5 kJ) has little effect on the initial temperature of Cl condensation, but T_{50} is reached much more rapidly, at about 600 K. To put these values in context, if chlorapatite is completely destabilised then T_{50} into KCl is about 420 K, while we would need to go to the lower limit of measured heats of formation to push T_{50} significantly above 620 K.

We used bromapatite heat of formation data from Cruz et al. (2005) and estimated the heat capacity and entropy of this phase from the values for fluorapatite, CaF_2 and $CaBr_2$. Based on these estimates, Br should not condense above 350 K in apatite. We instead calculate condensation at about 420 K into K(Cl,Br) solid solution. Activity coefficients for KBr, based on the low bulk modulus of KCl (Vijay and Verma 2000) should be about 3.36 at 420 K. Using the same elasticity data, KI should have an activity coefficient of ~7000 in KCl under these conditions, which means that the activity of KI dissolved in KCl would be much greater than 1. KI should therefore condense as a pure phase with T_{50} of 390 K.

4.2 Low temperature condensation into Fe and FeS

4.2.1 Nonideality issues. Lodders (2003) groups Ag, As, Au, Bi, Cu, Ge, P, Pb, Sb, Sn, and Te as siderophile elements condensing into the Fe alloy. We began by assuming ideal solution of most of these elements in the metal and found good agreement with Lodders' T_{50} values (in brackets), as follows As-1030 K (1065); Pb-739 K (727); Bi-751 K (746); Ag-997 K (996); Sb-930 K (979); Sn-725 K (704). The problem with these values, however, is that there are demonstrable nonidealities evidenced by the insolubility of, for example, Ag, Pb, and Bi in solid iron. When the activity coefficients implied by the low extents of solubility, as exemplified by Ag, discussed above, are added to the thermodynamic data, the condensation temperatures are depressed by several hundred K. Frequently, however, the effect is lessened by the precipitation of another phase, generally FeS, into which the trace element dissolves.

4.2.2 Condensation into iron: Au, As, Cu, Ge, Ga, Sb, and Bi. Au, which has AuS as the dominant gas species, has large activity coefficients in solid Fe (Boom et al. 1983). Nevertheless, we find condensation into Fe with T_{50} of 967 K. Arsenic dissolves into Fe with strong negative deviations from ideality. Both the Miedema model and a more recent thermodynamic assessment (Pei et al. 1994) lead to essentially the same T_{50} of 1235 K. Cu has small positive deviations from ideality when dissolved in Fe (Arita et al. 1981). We obtain virtually identical T_{50} to that of Lodders (2003) (1035K) when the nonidealities are accounted for. The condensation temperature of Ge into Fe is influenced by large negative deviations from ideal solution. We estimated the enthalpy of solution of Ge in Fe from the results of Predel and Vogelbein (1979) and converted this (-52 kJ/gm·atom) to activity coefficients using Equation (11). The result is similar to that of Wai and Wasson (1979), a calculated T_{50} temperature of 830 K. Ga also dissolves in Fe with strong negative deviations from ideality. The most stable gaseous species at low temperatures are GaCl, GaF and GaOH (Wai and Wasson 1979) although the free energy of GaOH is fairly uncertain (Battat et al. 1974). Taking account of the enthalpy of solution data for Ga in Fe (Predel and Vogelbein

1975) we obtain a T_{50} value of approximately 1010 K. The considerable uncertainty is highlighted if we use the Wai and Wasson (1979) estimate for γ_{Ga}. This would lower T_{50} by about 200 K.

For antimony, SbS should, given Knudsen cell mass spectrometric data (Hino et al. 1986), be an important gas species in the temperature range of interest, with Sb_2 , Sb^0 , Sb_4 and SbCl all present in proportions which are strongly temperature-dependent. We find that, given the activity coefficients estimated from phase relations (Pei et al. 1995) Sb condenses into iron at around 890 K. Use of the lower activity coefficients adopted by Wai and Wasson (1979) would raise this by ~100 K.

Sn may condense either into Fe metal or into FeS depending on activity coefficients. For the metal, we estimate a minimum activity coefficient of 45 at 873 K based on the Fe-Sn phase diagram (Hari Kumar et al. 1996) while in FeS an activity coefficient of 1060 is obtained at 700K from the lattice strain model given an E_s of 81 GPa (discussed below). The most stable gas species is SnS and the condensation temperature into Fe is 604 K while condensation into sulfide is calculated to be at about 50K lower temperature.

There is essentially complete immiscibility in the Bi-Fe system with activity coefficients of the order of 2500 even in liquid Fe at 1873 K (Boa et al. 2008). Extrapolating this value down to 750 K or using the Miedema model results in either case of Bi activity >1 in Fe. Hence Bi should precipitate as Bi metal rather than in solution in Fe. We obtain T_{50} of 485 K for Bi metal.

4.2.3 Condensation into FeS and as sulfide. S, Se and Te all condense primarily into FeS. The PHEQ program has thermodynamic data for both pyrrhotite $Fe_{0.877}S$ and troilite FeS which are treated as separate phases. Using the data as given, pyrrhotite should precipitate

460 first from a solar gas. This has been shown, however to be inconsistent with more recent
461 thermodynamic data (Grønvold and Stølen 1992; Lauretta et al. 1996). Lauretta et al (1996)
462 showed that, at the H_2S/H_2 ratio of the solar nebula, the thermodynamic data of Grønvold and
463 Stølen (1992) indicate that FeS, troilite should be the most stable sulfide and hence should
464 appear first. We therefore used the data of Grønvold and Stølen (1992) for FeS and $Fe_{0.875}S$ to
465 calculate that troilite appears at 710 K with T_{50} for S of 672 K, virtually identical to the
466 Lodders (2003) value for S.

467 We have measured (unpublished) partition coefficients of Se between solid FeS and
468 sulfide liquid of about 0.6 at 1293 K. We assume that this corresponds to the reciprocal of
469 the activity coefficient which is therefore 1.67 at 1293 K. The stable gas species H_2Se
470 condenses FeSe into FeS with T_{50} of 701 K. We used the same approach for Te and adopted
471 an activity coefficient of 40 at 1293 K based on our partitioning experiments. This results in
472 T_{50} of 665 K.

473 For Ag we assumed nonideal solution with activity coefficients obtained from the
474 lattice strain model and E_s of 81 GPa, which is in reasonable agreement with the bulk moduli
475 of the different FeS polymorphs (Kusaba et al. 1997) and with r_o the 6-fold radius of Fe^{2+}
476 (Shannon 1976). These parameters were also constrained to be in accord with our measured
477 (unpublished) solid sulfide-liquid sulfide partition coefficient D_{Ag} of ~0.03 at 1323 K. Ag is
478 calculated to condense into iron sulfide with T_{50} of 699 K.

479 The most stable gaseous species of Cd should be Cd^0 and this condenses into FeS
480 with a T_{50} of 502 K. Activity coefficients were obtained from the lattice strain model with
481 Cd^{2+} radius from Shannon (1976).

ZnS mixes with only small nonidealities into FeS (Fleet 1975) and we find that, incorporating Fleet's results, Zn condenses into FeS essentially as soon as it appears, with T_{50} of 704 K.

Indium has several important gaseous species in the temperature range of interest, including InOH (Skulan et al. 2006) and InCl (Barin 1989). The latter dominates before Cl condenses. Indium has stable sulfides InS and In_2S_3 and the former should be more stable at the H_2S fugacities of the solar nebula. Assuming that InS dissolves ideally in FeS, we obtain a T_{50} of 580K. In^{2+} is, however significantly larger than Fe^{2+} and InS has metal-metal bonds (Schwarz 2002; Schwarz et al. 1995) so is unlikely to dissolve ideally in FeS. The low pressure structure (Schwarz et al. 1995) has a very distorted coordination polyhedron around In, with average In-S distances of 2.92Å, which, taking the S^{2-} radius from Shannon (1976) leads to an In^{2+} radius of 1.08 Å. The polyhedron becomes much less distorted by 4.3 GPa however (Schwarz et al. 1995), and performing the same calculation leads to an In^{2+} radius of 0.92Å. We averaged these 2 values and used the lattice strain model to estimate an activity coefficient of 5.2 at 1000 K in FeS. We hence calculate that In will condense as InS into FeS at 492 K (T_{50}) from the solar gas. This temperature would decrease by ~25 K if we were to apply the lattice strain model and assume an ionic radius of In^{2+} of 1.08 Å. For HgS we used data on the pressure of Hg^0 plus S_2 over heated HgS (Ferro et al. 1989; Mills 1974) to calculate the conditions of HgS condensation into FeS. We took account of the nonidealities of HgS in FeS using the lattice strain model with E_s and r_0 as discussed above. The T_{50} condensation temperature is 240 K.

We used the lattice strain model for condensation of PbS into FeS and obtain an activity coefficient of 686 at 1000 K. This means that, at solar system abundances, PbS

activities in FeS would be >1 below 530 K. At lower temperatures Pb would condense from Pb^0 and H_2S as pure PbS. We thus obtain condensation of pure PbS at 495 K.

Tl behaves similarly to Pb. The lattice strain model gives activity coefficients on the order of 10^{10} at 1000 K for dissolution into FeS while the Miedema model gives activity coefficients of about 10^8 for dissolution into Fe metal at the same temperature. These large values mean that Tl should condense into a Tl phase, either Tl_2S or Tl metal and the temperatures are of the order of 400 K or lower depending on the stability of the TlCl gaseous species (Fig. 3). We find that the T_{50} temperatures for Tl condensing into both Tl metal and Tl_2S are virtually identical, at 365 K.

5. Condensation into silicates: K, Rb, Cs, Li, Mn, and B

The alkalis K, Rb and Cs were all assumed to condense into the phases with which they are most associated in nature, the feldspars. For K we assumed condensation into either the albitic plagioclase present in the major element condensation sequence or into a separate sanidine feldspar. We calculated activity coefficients in plagioclase using lattice strain parameters derived from plagioclase-liquid partitioning experiments (Blundy and Wood 1994) and obtained a T_{50} temperature of 993 K into plagioclase with K^0 as the dominant gas species. Given an activity coefficient of 35 from the lattice strain model at 700 K however, $KAlSi_3O_8$ should exsolve from plagioclase at lower temperature. Cs and Rb will then condense into sanidine. We modelled the properties of Rb and Cs feldspar by assuming that the log K of formation of $RbAlSi_3O_8$ minus that of $KAlSi_3O_8$ and of $CsAlSi_3O_8$ minus $KAlSi_3O_8$ are the same as the differences in log K of formation of $RbO_{0.5}$ minus $KO_{0.5}$ and of $CsO_{0.5}$ minus $KO_{0.5}$. Then we used the lattice strain model data (Blundy and Wood 1994) to calculate activity coefficients for dissolution into sanidine. This yields T_{50} values of 752 K for Rb and 593 K for Cs.

The dominant gas species of Li close to the condensation temperature is LiCl. We used the orthopyroxene-liquid partition coefficient data (Frei et al. 2009) to estimate an activity coefficient of ~5. Assuming that Li dissolves in pyroxene as Li_2SiO_3 we obtain T_{50} of 1148 K. If we were to treat Li_4SiO_4 dissolution into olivine in a similar manner we would obtain a lower condensation temperature. According to the partitioning data of Frei et al. (2009) Mn^{2+} fits into the M2 site of orthopyroxene without strain ($\gamma = 1.0$) and will fit into the M1 site with an activity coefficient of 1.5 at 1673 K. Given the close approach to ideality and D_{Mn} (liquid/crystal) values close to 1.0 (Laubier et al. 2014; Le Roux et al. 2015) for both orthopyroxene and olivine we assumed that Mn mixes ideally in olivine and Mg-pyroxene during condensation. We obtain virtually identical temperatures for condensation into pyroxene and olivine (1123 K). This is reduced by 11 K if we make explicit provision for the small nonidealities mentioned above.

In the low temperature region of interest B_2O_3 is calculated to be the most stable form of B in both gas and solid phases and, assuming, following Lodders (2003) that B replaces Al in plagioclase feldspar, then, if the solution is ideal, we obtain T_{50} of 740 K.

6. Discussion

The results of our calculations are given in Table 2 together with a summary of the activity coefficient expressions discussed above. Figure 4 shows silicate Earth abundances of the elements plotted, in the same manner as in Figure 1, versus the T_{50} condensation temperatures generated in this study. One might argue that, with the exception of the elements S, Se, and Te, the "volatility trend" is better defined by our results than by those of Lodders (2003). This would require either the "eye of faith" or a statistical analysis which we do not consider worth performing, however, since there is no physical or chemical reason we are aware of that the volatile elements should all fall on the same line in a plot of this kind.

Planetary and protoplanetary processes such as melting, core formation and silicate differentiation must obviously have exerted considerable influence on the final abundances of elements in silicate Earth.

Figure 5a shows the differences between our values of T_{50} and those of Lodders (2003). As can be seen, agreement is good for the relatively refractory elements which condense above 1300 K. Principal differences are found at temperatures below 900 K where we find Cl-species stable in the gas phase and strong nonidealities in the solid phases for most elements. Both these effects reduce condensation temperature leading to a positive difference between Lodders' condensation temperatures and ours.

7. Conclusions and implications

We have attempted to update the generally-accepted equilibrium condensation temperatures of Lodders (2003) by making what we believe are realistic assumptions about activity coefficients for trace elements dissolved in the major phases, Fe, FeS, pyroxene, olivine, and plagioclase. In the course of this re-analysis we also found, based on reversed phase equilibrium experiments (Sharp et al. 1989) that the stability of sodalite during the condensation sequence is much lower than was proposed in the earlier study. This means that the T_{50} temperature for Cl is 472 K rather than 948 K. The presence of significant amounts of cosmochemically abundant Cl (as HCl) in the gas phase between 1000 and 400 K stabilises gaseous chlorides such as KCl, RbCl, CsCl, GaCl, TlCl, and InCl and lowers condensation temperatures for these minor elements.

One important point to note is that some earlier authors (Grossman 1972; Grossman and Larimer 1974; Larimer 1967; Wai and Wasson,1979) made solid solution assumptions and used gaseous species which are similar to the ones we find to be most appropriate. Hence their results are frequently close to ours, as can be seen in Figure 5b and Table 2. These

authors only studied small subsets of the periodic table, however, and the more recent all-encompassing study of Lodders (2003) has superseded their work in the minds of most geochemists. We believe that our critique and discussion here will provide more context for condensation results and give the reader some idea of where there are significant uncertainties or errors in the calculations.

In conclusion we must recognise that it is impossible to generate a list of **exact** condensation temperatures of the elements from a solar gas. There are uncertainties in solar abundances, uncertainties in the thermodynamic data that we use and, at low temperatures at least, in the assumption that perfect equilibrium is maintained and that all stable solids have been considered. However, given the equilibrium assumption, we do assert that we have a robust list. We await with interest for future updates and comments on our work.

Acknowledgements

This work would have been much more arduous if John Wood had not provided BJW with the source code and database for PHEQ about 25 years ago. He is gratefully acknowledged. TH commenced this work as a 4th year undergraduate project. We received funding from the European Research Council grant 267764 and from the Natural Environment Research Council (UK) grant NE/M000427/1. We acknowledge with thanks the detailed and constructive reviews of Andrew Davis, Denton Ebel, Mikhail Petaev and Laura Schaefer, particularly the fact that the last 2 reviewers repeated and checked some of our calculations. Any remaining errors and omissions are of course entirely our responsibility.

References

598 Arita, M., Tanaka, M., Goto, K.S., and Someno, M. (1981) Activity and diffusivity
599 measurements of copper in gamma and delta Fe by equilibration between solid Fe and liquid
600 Ag. Metallurgical and Materials Transactions A, 12, 497-504.

601 Barin, I., Sauert, F., Schultze-Rhonhof, E., and Sheng, W.S. (1989) Thermochemical data of
602 pure substances, Part I and Part II. CH Verlagsgesellschaft, Weinheim, Germany.

603 Battat, D., Faktor, M.M., Garrett, I., and Moss, R.H. (1974) Modified entrainment method for
604 measuring vapor-pressures and heterogeneous equilibrium-constants .2. Equilibria in water-
605 gallium system. Journal of the Chemical Society-Faraday Transactions, 70, 2280-2292.

606 Blundy, J.D., and Wood, B.J. (1994) Prediction of crystal–melt partition coefficients from
607 elastic moduli. Nature, 372, 452-454.

608 Boa, D., Hassam, S., Krac, G., Kotchi, K.P. and Rogez, J. (2008) The ternary bismuth-iron-
609 antimony system: Experimental phase diagram study and thermodynamic evaluation.
610 Calphad-Computer Coupling of Phase Diagrams and Thermochemistry, 32, 227-239.

611 Boom, R., De Boer, F.R., Niessen, A.K., and Miedema, A.R. (1983) Enthalpies of formation
612 of liquid and solid binary alloys based on 3d metals III. Alloys of Iron. Physica B, 115B, 285-
613 309.

614 Brice, J.C. (1975) Some thermodynamics aspects of the growth of strained crystals. Journal
615 of Crystal Growth, 28, 249-253.

616 Chase, M.W. Jr., Davies, C.A., Downey, J.R.Jr.,Frurip,D.J., McDonald, R.A., and Syverud,
617 A.N. (1985) JANAF Thermochemical Tables Third Edition. Journal of Physical and
618 Chemical Reference Data 14, Supplement 1, 1856 pp

Clay, P.L., Burgess, R., Busemann, H., Ruzie-Hamilton, L., Joachim, B., Day, J.M.D., and Ballentine, C.J. (2017) Halogens in chondritic meteorites and terrestrial accretion. Nature, 551, 614-618.

Corgne, A. and Wood, B.J. (2005) Trace element partitioning and substitution mechanisms in calcium perovskites. Contributions to Mineralogy and Petrology 149, 85-97.

Cruz, F., da Piedade, M.E.M., and Calado, J.C.G. (2005) Standard molar enthalpies of formation of hydroxy-, chlor-, and bromapatite. Journal of Chemical Thermodynamics, 37, 1061-1070.

Davis, A.M., Zhang, J., Greber, N.D., Hu, J., Tissot, F.L.H., and Dauphas, N. (2018) Titanium isotopes and rare earth patterns in CAI's: Evidence for thermal processing and gas-dust decoupling in the protoplanetary disk. Geochimica et Cosmochimica Acta 221, 275-295.

Del Bucchia, S., Jumas, J.-C., and Maurin, M. (1981) Contribution à l'Etude de Composés Sulfurés d'Etain(II): Affinement de la Structure de SnS. Acta Crystallographica B, 37, 1903-1905.

Dreibus, G., and Palme, H. (1996) Cosmochemical constraints on the sulfur content in the Earth's core. Geochimica et Cosmochimica Acta, 60, 1125-1130.

Drouet, D. (2015) A comprehensive guide to experimental and predicted thermodynamic properties of phosphate apatite minerals in view of applicative purposes. Journal of Chemical Thermodynamics 81, 143-159.

Evans, N.J., Dunham, M.M., Jorgensen, J.K., Enoch, M.L., Merin, B., van Dishoeck, E.F., Alcala, J.M., Myers, P.C., Stapelfeldt, K.R., Huard, T.L., Allen, L.E., Harvey, P.M., van Kempen, T., Blake, G.A., Koerner, D.W., Mundy, L.G., Padgett, D.L., and Sargent, A.I.

(2009) The Spitzer c2d Legacy results: star-formation rates and efficiencies; evolution and lifetimes. The Astrophysical Journal Supplement Series, 181, 321-350.

Ferro, D., Piacente, V., and Scardala, P. (1989) Vaporization enthalpies of black and red mercury sulfides and their heat of transition from vapor-pressure measurements. Journal of the Less-Common Metals, 147, 1-8.

Fleet, M.E. (1975) Thermodynamic properties of (Zn,Fe)S solid solutions at 850ºC. American Mineralogist, 60, 466-470.

Frei, D., Liebscher, A., Franz, G., Wunder, B., Klemme, S., and Blundy, J. (2009) Trace element partitioning between orthopyroxene and anhydrous silicate melt on the lherzolite solidus from 1.1 to 3.2 GPa and 1230 to 1535 degrees C in the model system Na_2O-CaO-MgO-Al_2O_3-SiO_2. Contributions to Mineralogy and Petrology, 157, 473-490.

Glushko, V. P., Gurvich, L. V., Bergman, G. A., Veitz, I. V., Medvedev, V . A., Khachkuruzov, G. A., and Jungman,V . S. (1978) Thermodynamic Properties of Pure Substances, 3rd ed. Nauka Publishers.

Grimsey, E.J., and Biswas, A.K. (1977) The activity of iron in low-iron liquid (Ni + Au + Fe) and solid (Ni + Fe) alloys at 1573 K. The Journal of Chemical Thermodynamics 9, 415-422.

Grønvold, F., and Stølen, S. (1992) Thermodynamics of iron sulfides II. Heat capacity and thermodynamic properties of FeS and of $Fe_{0.875}S$ at temperatures from 298.15 K to 1000 K, of $Fe_{0.98}S$ from 298.15 K to 800 K, and of $Fe_{0.89}S$ from 298.15 K to about 650 K. Thermodynamics of formation. Journal of Chemical Thermodynamics 24, 913-936.

Grossman, L. (1972) Condensation in the primitive solar nebula. Geochimica et Cosmochimica Acta, 36, 597-619.

Grossman, L., and Larimer, J.W. (1974) Early chemical history of the solar-system. Reviews of Geophysics, 12, 71-101.

Hashimoto, A. (1992) The effect of H_2O gas on volatilities of planet-forming major elements: I. Experimental determination of thermodynamic properties of Ca-, Al- and Si-hydroxide gas molecules, and its application to the solar nebula. Geochimica et Cosmochimica Acta 56, 511-532.

Hari Kumar, K.C., Wollants, P., and Delaey, L. (1996) Thermodynamic evaluation of the Fe-Sn phase diagram. Calphad, 20, 139-149.

Helgeson, H.C., Delany, J.M., Nesbitt, H.W., and Bird, D.K. (1978) Summary and critique of the thermodynamic properties of rock-forming minerals. American Journal of Science, 278, 1-229.

Hino, M., Nagamori, M., and Toguri, J.M. (1986) Thermodynamics of gaseous SbS. Metallurgical Transactions B 17, 913-914.

Hovis, G.L., and Harlov, D.E. (2010) Solution calorimetric investigation of fluor-chlorapatite crystalline solutions. American Mineralogist, 95, 946-952.

Kiseeva, E.S., and Wood, B.J. (2013) A simple model for chalcophile element partitioning between sulphide and silicate liquids with geochemical applications. Earth and Planetary Science Letters, 383, 68-81.

Knacke, O., Kubaschewski, O., and Hessemann, K. (1991) Thermochemical Properties of Inorganic Substances (2nd ed.) Vol I & II. Springer, Berlin.

Komada, N., Westrum, E.F., Hemingway, B.S., Zolotov, M.Y., Semenov, Y.V., Khodakovsky, I.L., and Anovitz, L.M. (1995) Thermodynamic properties of sodalite at temperatures from 15 K to 1000 K. Journal of Chemical Thermodynamics, 27, 1119-1132.

Konings, R.J.M., Benes, O., Kovacs, A., Manara, D., Sedmidubsky, D., Gorokhov, L., Iorish, V.S., Yungman, V., Shenyavskaya, E., and Osina, E. (2014) The Thermodynamic Properties of the f- Elements and their Compounds. Part 2. The Lanthanide and Actinide Oxides. Journal of Physical and Chemical Reference Data, 43.

Kumar, R.V., and Kay, D.A.R. (1985) The utilization of galvanic cells using Ca b-alumina solid electrolytes in a thermodynamic investigation of the CaO-Al_2O_3 system. Metallurgical Transactions 16B, 107-112.

Kusaba, K., Syono, Y., Kikegawa, T., and Shimomura, O. (1997) The structure of FeS under high pressure. Journal of Physics and Chemistry of Solids, 241-246.

Larimer, J.W. (1967) Chemical fractionations in meteorites-I. Conensation of elements. Geochimica et Cosmochimica Acta, 31, 1215-1238.

Laubier, M., Grove, T.L., and Langmuir, C.H. (2014) Trace element mineral/melt partitioning for basaltic and basaltic andesitic melts: An experimental and laser ICP-MS study with application to the oxidation state of mantle source regions. Earth and Planetary Science Letters, 392, 265-278.

Lauretta, D.S., Kremser, D.T., and Fegley, B.J. (1996) The Rate of Iron Sulfide Formation in the Solar Nebula. Icarus 122, 288-315.

Le Roux, V., Dasgupta, R., and Lee, C.T.A. (2015) Recommended mineral-melt partition coefficients for FRTEs (Cu), Ga, and Ge during mantle melting. American Mineralogist, 100, 2533-2544.

Lewis, J.S., and Prinn, R.G. (1980) Kinetic inhibition of CO and N_2 reduction in the solar nebular. The Astrophysical Journal 238, 357-364.

Lodders, K. (1999) Revised thermochemical properties of phosphinidene (PH), phosphine (PH_3), phosphorus nitride (PN) and magnesium phosphate ($Mg_3P_2O_8$). Journal of Physical and Chemical Reference Data 28, 1705-1712.

Lodders, K. (2003) Solar system abundances and condensation temperatures of the elements. The Astrophysical Journal, 591, 1220-1247.

Lodders, K. (2004) Revised and updated thermochemical properties of the gases mercapto (HS), disulfur monoxide (S_2O) Thiazyl (NS) and Thioxophosphino (PS). Journal of Physical and Chemical Reference Data 33, 357-367.

Mel'chakova, L.V., Ogorodova, L.P., and Kiseleva, I.A. (2004) The enthalpy of dormation and heat capacity of phlogopite. Russian Journal of Physical Chemistry 78, 860-863.

Miedema, A.R., De Chatel, P.F., and De Boer, F.R. (1980) Cohesion in Alloys-Fundamentals of a semi-empirical model. Physica, 100B, 1-28.

Mills, K.C., 1974. Thermodynamic data for Inorganic Sulphides, Selenides and Tellurides. Butterworths, London.

Nagasawa, H., Schreiber, H.D., and Morris, R.V. (1980) Experimental mineral-liquid partition-coefficients of the rare-earth elements (REE), Sc and Sr for perovskite, spinel and melilite. Earth and Planetary Science Letters, 46, 431-437.

726 Orville, P.M. (1972) Plagioclase cation exchange equilibria with aqueous chloride solution at
727 700°C and 2000 bars in the presence of quartz. American Journal of Science 272, 234-272

728 Palme, H., and O'Neill, H. (2014) Cosmochemical Estimates of Mantle Composition,
729 Treatise on geochemistry volume 3, second ed. Elsevier, pp. 1-39.

730 Pedley, J.B., and Marshall, E.M. (1983) Thermochemical data for gaseous monoxides.
731 Journal of Physical and Chemical Reference Data, 12, 967-1031.

732 Pei, B.Y., Bjorkman, B., Jansson, B., and Sundman, B. (1994) Thermodynamic assessment of
733 the Fe-As system using as ionic 2-sublattice model for the liquid-phase. Zeitschrift Fur
734 Metallkunde, 85, 171-177.

735 Pei, B.Y., Bjorkman, B., Sundman, B., and Jansson, B. (1995) A thermodynamic assessment
736 of the iron – antimony system. Calphad-Computer Coupling of Phase Diagrams and
737 Thermochemistry, 19, 1-15.

738 Petaev, M.I. (2009) The GRAINS thermodynamic and kinetic code for modeling nebular
739 condensation. Calphad-computer coupling of phase diagrams and thermochemistry, 33, 317-
740 327.

741 Predel, B., and Vogelbein, W. (1975) Thermodynamische untersuchung der systeme eisen-
742 gallium und kobalt-gallium. Thermochim Acta ,13, 133-145.

743 Predel, B., and Vogelbein, W. (1979) Bildungsenthalpien fester legierungen der binären
744 systeme des eisens, kobalts und nickels mit germanium und zinn. Thermochim Acta, 30, 201-
745 215.

Righter, K., Hervig, R.L., and Kring, D.A. (1998) Accretion and core formation on Mars: Molybdenum contents of melt inclusion glasses in three SNC meteorites. Geochimica et Cosmochimica Acta, 62, 2167-2177.

Robie, R.A., Hemingway, B.S., and Fisher, J.R. (1978) Thermodynamic properties of minerals and related substances at 298.15 K and 1 bar (105 Pascals) pressure and at higher temperatures, Washington, D.C.

Roszjar, J., Whitehouse, M.J., Srinivasan, G., Mezger, K., Scherer, E.E., Van Orman, J.A., and Bischoff, A. (2016) Prolonged magmatism on 4 Vesta inferred from Hf-W analyses of eucrite zircon. Earth and Planetary Science Letters, 452, 216-226.

Schwarz, U. (2002) Crystal structure of indium monosulfide, InS, at 7.9 GPa. Zeitschrift für Kristallographie – New Crystal Structures, 217, 470-470.

Schwarz, U., Hillebrecht, H., and Syassen, K. (1995) Effect of hydrostatic pressures on the crystal structure of InS. Zeitschrift für Kristallographie, 210, 494-497.

Shannon, R.D. (1976) Revised ionic radii and systematic studies of interatomic distances in halides and chalcogenides. Acta Crystallographica Section A, A-32, 751-767.

Sharp, Z.D., Helffrich, G.R., Bohlen, S.R., and Essene, E.J. (1989) The stability of sodalite in the system $NaAlSiO_4$-NaCl. Geochimica et Cosmochimica Acta, 53, 1943-1954.

Skulan, A., Nielsen, I., Melius, C., and Allendorf, M. (2006) BAC-MP4 predictions of thermochemistry for gas-phase indium compounds in the In-H-C-O-Cl system. The Journal of Physical Chemistry A, 110, 281-290.

Steelmaking Data Sourcebook (1988). Gordon and Breach, New York 325pp.

767 Stormer, J.C., and Carmichael, I.S.E. (1971) The free energy of sodalite and the behavior of
768 chloride, fluoride and sulfate in silicate magmas. American Mineralogist, 56, 292-306.

769 Vijay, A., and Verma, T.S. (2000) Analysis of temperature dependence of elastic constants
770 and bulk modulus for ionic solids. Physica B 291, 373-378.

771 Wai, C.M., and Wasson, J.T. (1979) Nebular Condensation of Ga, Ge and Sb and the
772 Chemical Classification of Iron-Meteorites. Nature, 282, 790-793.

773 Wasson, J.T. (1985) Meteorites, Their Record of Early Solar-system history. W.H. Freeman,
774 New York.

775 Wellman, T.R. (1969) The vapor pressure of NaCl over decomposing sodalite. Geochimica et
776 Cosmochimica Acta, 33, 1302-1304.

777 Witt-Eickschen, G., Palme, H., O'Neill, H.S.C., and Allen, C.M. (2009) The geochemistry of
778 the volatile trace elements As, Cd, Ga, In and Sn in the Earth's mantle: New evidence from in
779 situ analyses of mantle xenoliths. Geochimica et Cosmochimica Acta, 73, 1755-1778.

780 Wood, B.J. (1993) Carbon in the core. Earth and Planetary Science Letters, 117, 593-607.

781 Wood, B.J., Kiseeva, E.S., and Mirolo, F.J. (2014) Accretion and core formation: The effects
782 of sulfur on metal-silicate partition coefficients. Geochimica et Cosmochimica Acta, 145,
783 248-267.

784 Wood, B.J., Walter, M.J., and Wade, J. (2006) Accretion of the Earth and segregation of its
785 core. Nature, 441, 825-833.

786 Wood, J.A., and Hashimoto, A. (1993) Mineral equilibrium in fractionated nebular systems.
787 Geochimica et Cosmochimica Acta, 57, 2377-2388.

788 Wriedt, H.A., Morrison, W.B., and Cole, W.E. (1973) Solubility of Silver in Gamma-Fe.
789 Metallurgical Transactions, 4, 1453-1456.

790 Zaitsev, A.I., Dobrokhotova, Z.V., Litvina, A.D., and Mogutnov, B.M. (1995)
791 Thermodynamic properties and phase equilibria in the Fe-P system. Journal of the Chemical
792 Society, Faraday Transactions 91, 703-712.

793 **Figure Captions**

794 Figure 1: Graph of abundance of elements in the silicate Earth, relative those in CI chondrites
795 (Palme and O'Neill 2014), normalised to Mg = 1.0, plotted versus the calculated temperature
796 (Lodders 2003) at which 50% of the element would be condensed from a gas of solar
797 composition at 10^{-4} bar.

798 Figure 2: (a) Fractions of different phases present in the stable solid assemblage as a function
799 of temperature at total pressure = 10^{-4} bar. Corundum is the first phase to appear at about
800 1680 K and is joined by small amounts of hibonite and melilite before the major phase of
801 condensation begins at ~1380 K. (b) Concentrations of major elements in the gas phase
802 (normalised to the initial Mg content of the solar gas) as a function of temperature at 10^{-4} bar.

803 Figure 3: Showing the ratio of MCl to M^0 in the gas phase as a function of temperature for a
804 number of elements of interest. Total pressure of 10^{-4} bar and partial pressure of HCl
805 computed at each temperature by free energy minimisation using the PHEQ program.

806 Figure 4: Abundances of elements in the silicate Earth, relative those in CI chondrites (Palme
807 and O'Neill 2014), normalised to Mg = 1.0, plotted versus the calculated temperatures (this
808 work) at which 50% of each element would be condensed from a gas of solar composition at
809 10^{-4} bar.

Figure 5: A comparison of our results for 50% condensation temperatures of the elements (T_{50}) to those of (a.) Lodders (2003) and (b.) Wasson (1985). Principal differences arise for the volatile elements because of the stabilities of Cl complexes in the gas phase and the nonidealities of trace elements in Fe(metal) and iron sulfide (see text).

Table 1: Major solid and gaseous species present at different temperatures and fugacities of O_2, H_2O, H_2S and HCl

Temperature (K)	Pressure (bar)	log (fO_2)	log (fH_2O)	log (fH_2S)	log (fHCl)	Major Gas Species (> 1 ppm)	Major Solid Phases
1700	1.00×10^{-4}	-15.99	-7.31	-9.30	-11.14	Al, CO, Ca, Fe, He, H_2, H_2O, H, H_2S, Mg, Na, SiO, S, SiS, SH, N_2, Ni	
1650	1.00×10^{-4}	-16.45	-7.31	-9.14	-11.14	Al, CO, Ca, He, Fe, H_2, H_2O, H, H_2S, Mg, Na, SiO, S, SiS, SH, N_2, Ni	Cnr
1600	1.00×10^{-4}	-16.94	-7.31	-9.00	-11.13	CO, Ca, Fe, He, H_2, H_2O, H, H_2S, Mg, Na, SiO, S, SiS, SH, N_2, Ni	Hbn
1550	1.00×10^{-4}	-17.46	-7.31	-8.89	-11.14	CO, Ca, Fe, He, H_2, H_2O, H, H_2S, Mg, Na, SiO, S, SiS, SH, N_2, Ni	Mll, Hbn
1500	1.00×10^{-4}	-18.01	-7.31	-8.80	-11.13	CO, Fe, He, H_2, H_2O, H, H_2S, Mg, Na, SiO, S, SiS, SH, N_2, Ni	Cnr, Mll
1450	1.00×10^{-4}	-18.60	-7.31	-8.74	-11.13	CO, Fe, He, H_2, H_2O, H, H_2S, Mg, Na, SiO, S, SiS, SH, N_2, Ni	Cnr, Mll
1400	1.00×10^{-4}	-19.23	-7.31	-8.70	-11.13	CO, Fe, He, H_2, H_2O, H, H_2S, Mg, Na, SiO, SiS, SH, N_2, Ni	Spl, Mll
1350	1.00×10^{-4}	-19.98	-7.35	-8.67	-11.14	CO, Fe, He, H_2, H_2O, H, H_2S, Mg, Na, SiO, SiS, SH, N_2	Ol, Spl, Cpx, Mll, Fe-alloy
1300	1.00×10^{-4}	-20.89	-7.44	-8.61	-11.14	CO, Fe, He, H_2, H_2O, H, H_2S, Mg, Na, SiO, SiS, SH, N_2	Ol, Cpx, Pl, Fe-alloy, Scb
1250	1.00×10^{-4}	-21.77	-7.49	-8.55	-11.15	CO, Fe, He, H_2, H_2O, H, H_2S, Na, SiO, SiS, SH, N_2	Ol, Opx, Cpx, Pl, Fe-alloy, Scb, Sa
1200	1.00×10^{-4}	-22.65	-7.50	-8.52	-11.17	CO, He, H_2, H_2O, H, H_2S, Na, N_2	Ol, Opx, Cpx, Pl, Fe-alloy, Scb, Sa
1150	1.00×10^{-4}	-23.58	-7.50	-8.52	-11.22	CO, He, H_2, H_2O, H, H_2S, Na, N_2	Ol, Opx, Cpx, Pl, Fe-alloy, Scb, Sa
1100	1.00×10^{-4}	-24.59	-7.50	-8.52	-11.33	CO, He, H_2, H_2O, H, H_2S, Na, N_2	Ol, Opx, Cpx, Pl, Fe-alloy, Scb, Sa
1050	1.00×10^{-4}	-25.70	-7.50	-8.51	-11.49	CO, He, H_2, H_2O, H_2S, Na, N_2	Ol, Opx, Cpx, Pl, Fe-alloy, Scb, Sa
1000	1.00×10^{-4}	-26.92	-7.50	-8.51	-11.56	CO, He, H_2, H_2O, H_2S, N_2	Ol, Opx, Cpx, Pl, Fe-alloy, Scb, Sa
950	1.00×10^{-4}	-28.27	-7.50	-8.51	-11.53	CO, He, H_2, H_2O, H_2S, N_2	Ol, Opx, Cpx, Pl, Fe-alloy, Scb, Sa
900	1.00×10^{-4}	-29.77	-7.50	-8.51	-11.40	CO, He, H_2, H_2O, H_2S, N_2	Ol, Opx, Cpx, Pl, Fe-alloy, Scb, Sa
850	1.00×10^{-4}	-31.44	-7.50	-8.51	-11.28	CO, He, H_2, H_2O, H_2S, N_2	Ol, Opx, Cpx, Pl, Fe-alloy, Scb, Sa
800	1.00×10^{-4}	-33.32	-7.50	-8.51	-11.20	CO, He, H_2, H_2O, H_2S, N_2	Ol, Opx, Cpx, Pl, Fe-alloy, Scb, Sa
750	1.00×10^{-4}	-35.45	-7.50	-8.51	-11.15	CH_4, CO, CO_2, He, H_2, H_2O, H_2S, N_2	Ol, Opx, Cpx, Pl, Fe-alloy, Scb, Sa
700	1.00×10^{-4}	-37.79	-7.45	-8.61	-11.14	CH_4, CO, CO_2, He, H_2, H_2O, H_2S, N_2	Ol, Opx, Cpx, Pl, Fe-alloy, Tro, Scb, Sa
650	1.00×10^{-4}	-40.17	-7.24	-8.99	-11.13	CH_4, CO, CO_2, He, H_2, H_2O, H_2S, N_2	Ol, Spl, Opx, Cpx, Pl, Fe-alloy, Tro, Ap, Scb, Sa
600	1.00×10^{-4}	-43.11	-7.07	-9.43	-11.14	CH_4, CO, He, H_2, H_2O, H_2S, N_2	Ol, Spl, Opx, Cpx, Pl, Fe-alloy, Tro, Ap, Scb, Sa
550	1.00×10^{-4}	-46.96	-7.05	-9.97	-11.27	CH_4, He, H_2, H_2O, H_2S, N_2	Ol, Spl, Opx, Cpx, Pl, Fe-alloy, Tro, Ap, Sa
500	1.00×10^{-4}	-51.62	-7.06	-10.60	-11.37	CH_4, He, H_2, H_2O, N_2	Ol, Spl, Opx, Cpx, Pl, Fe-alloy, Tro, Ap, Sa
450	1.00×10^{-4}	-57.32	-7.06	-11.19	-11.54	CH_4, He, H_2, H_2O, N_2, NH_3	Ol, Spl, Opx, Cpx, Pl, Fe-alloy, Tro, Ap, Sa
400	1.00×10^{-4}	-64.43	-7.06	-11.84	-11.82	CH_4, He, H_2, H_2O, N_2, NH_3	Ol, Spl, Cpx, Pl, Tr, Fe-alloy, Tro, Ap, Sa
350	1.00×10^{-4}	-73.57	-7.07	-13.00	-19.07	CH_4, He, H_2, H_2O, N_2, NH_3	Ol, Spl, Cpx, Pl, Tr, Fe-alloy, Tro, Sdl, Ap, Sa

Crn - corundum; Hbn - hibonite; Mll - melilite; Spl - spinel; Ol - olivine; Cpx - clinopyroxene; Pl - plagioclase; Opx - orthopyroxene; Scb - schreibersite; Tro - troilite; Ap - apatite; Sdl - sodalite; Sa - sanidine

Table 2: 50% condensation temperatures and major host phases at 10^{-4} bar

Element	This Study			Lodders (2003)		Wasson (1985)
	T_{50} (K)	Phase	Activity coefficient (γ)	T_{50} (K)	Phase	T_{50} (K)
H						
He						
Li	1148	En	5.0 [1]	1142	Fo + En	1225
Be	1551	Mll	$\ln\gamma = 1000\cdot\ln(16)/T$ [2]	1452	Mll	
B	740	Pl	1 (assumed ideal)	908	Fsp	
C				40	$CH_4\cdot 7H_2O + CH_4$ ice	
N				123	$NH_3\cdot H_2O$	
O	183	Rock + Water ice		180	Rock + Water ice	
F	674	F-Ap	1 (assumed ideal)	734	F-Ap	736
Ne				9.1	Ne ice	
Na	1035	Pl	$\ln\gamma = (0.64\cdot X_{An})$, $X_{An} > 0.56$ ELSE 0 [3]	958	Fsp	970
Mg	1343	Fo + Cpx	1 (pure)	1336	Fo	1340
Al	1652	Crn	1 (pure)	1653	Hbn	1650
Si	1314	Fo + Cpx	1 (pure)	1310	Fo + En	1311
P	1287	Scb	1 (pure)	1229	Scb	1151
S	672	Tro	1 (pure)	664	Tro	648
Cl	472	Cl-Ap	1 (assumed ideal)	948	Sdl	863
Ar				47	$Ar\cdot 6H_2O$	
K	993	Pl	$\ln\gamma = 1100\cdot\ln(9.57)/T$ [2]	1006	Fsp	1000
Ca	1535	Mll	1 (pure)	1517	Hbn + Mll	1518
Sc	1541	Prv + Mll	1 (assumed ideal)	1659	Hbn	1644
Ti	1565	Prv	1 (pure)	1582	Prv	1549
V	1370	Fe alloy + Prv	$\ln\gamma = -29000/(8.314\cdot T)$ [4]	1429	Prv	1450
Cr	1291	Fe alloy	$\ln\gamma = -6000/(8.314\cdot T)$ [4]	1296	Fe alloy	1277
Mn	1123	Fo + En	1 (close to ideal) [1]	1158	Fo + En	1190
Fe	1338	Fe alloy	1 (assumed ideal)	1334	Fe alloy	1336
Co	1354	Fe alloy	0.85[4]	1352	Fe alloy	1351
Ni	1363	Fe alloy	0.68 [5]	1353	Fe alloy	1354
Cu	1034	Fe alloy	$\ln\gamma = 1000\cdot\ln(117)/T$ [7]	1037	Fe alloy	1037
Zn	704	Tro	$\ln\gamma = 1123\cdot\ln(1.86)/T$ [8]	726	Fo + En	660
Ga	1010	Fe alloy	$\ln\gamma = -7045/T$ [9]	968	Fe alloy + Fsp	918
Ge	830	Fe alloy	$\ln\gamma = -52000/(8.314\cdot T)$ [10]	883	Fe alloy	825
As	1235	Fe alloy	$\ln\gamma = -68000/(8.314\cdot T)$ [4]	1065	Fe alloy	1157
Se	701	Tro	$\ln\gamma = 1293\cdot\ln(1.67)/T$ [2]	697	Tro	684
Br	420	Syl	$\ln\gamma = 420\cdot\ln(3.36)/T$ [2]	546	Cl-Ap	~690
Kr				52	$Kr\cdot 6H_2O$	
Rb	752	Sa	$\ln\gamma = 1000\cdot\ln(1.43)/T$ [2]	800	Fsp	~1080
Sr	1548	Prv	$\ln\gamma = 1100\cdot\ln(1.53)/T$ [2]	1464	Ca-titanate	
Y	1551	Mll + Prv	1 (assumed ideal)	1659	Hbn	1592
Zr	1722	ZrO_2	1 (pure)	1741	ZrO_2	~1780
Nb	1561	Prv	1 (assumed ideal)	1559	Ca-titanate	~1550
Mo	1520	Mo metal	1 (pure)	1590	Refractory metal alloy	1608
Ru	1533	Os-Ir-Ru alloy	1 (assumed ideal)	1551	Refractory metal alloy	1573
Rh	1370	Fe alloy	$\ln\gamma = -23000/(8.314\cdot T)$ [4]	1392	Refractory metal alloy	1391
Pd	1330	Fe alloy	$\ln\gamma = -19000/(8.314\cdot T)$ [4]	1324	Fe alloy	1334
Ag	699	Tro	$\ln\gamma = 1323\cdot\ln(50)/T$ [2]	996	Fe alloy	952
Cd	502	Tro	$\ln\gamma = 1000\cdot\ln(2.6)/T$ [2]	652	En + Tro	430*
In	492	Tro	$\ln\gamma = 1000\cdot\ln(5.2)/T$ [2]	536	Tro	456*
Sn	604	Fe alloy	$\ln\gamma = 873\cdot\ln(45)/T$ [11]	704	Fe alloy	720
Sb	890	Fe alloy	$\ln\gamma = 1100\cdot\ln(1.7)/T$ [12]	979	Fe alloy	912
Te	665	Tro	$\ln\gamma = 1293\cdot\ln(40)/T$ [2]	709	Fe alloy	680
I	390	KI	1 (pure)	535	Cl-Ap	
Xe				68	$Xe\cdot 6H_2O$	
Cs	593	Sa	$\ln\gamma = 1000\cdot\ln(7.12)/T$ [2]	799	Fsp	
Ba	1423	Prv	$\ln\gamma = 1100\cdot\ln(64)/T$ [2]	1455	Ca-titanate	
La	1615	Hbn	0.164 [6]	1578	Hbn + Ca-titanate	1520
Ce	1454	Mll+ Prv	1 (assumed ideal)	1478	Hbn + Ca-titanate	1500
Pr	1550	Hbn + Prv	0.229 (Hbn) [6]	1582	Hbn + Ca-titanate	1532
Nd	1630	Hbn	0.297[6]	1602	Hbn	1510
Sm	1545	Hbn + Prv	0.55 (Hbn) [6]	1590	Hbn + Ca-titanate	1515
Eu	1491	Mll + Prv	1.28 [2]	1356	Hbn + Ca-titanate + Fsp	1450
Gd	1630	Hbn	1.1 [6]	1659	Hbn	1545
Tb	1630	Hbn	1.63 [6]	1659	Hbn	1560
Dy	1630	Hbn	2.49 [6]	1659	Hbn	1571
Ho	1630	Hbn	3.83 [6]	1659	Hbn	1568
Er	1630	Hbn	5.93 [6]	1659	Hbn	1590
Tm	1630	Hbn	9.37 [6]	1659	Hbn	1545
Yb	1528	Mll + Prv	1 (assumed ideal)	1487	Hbn + Ca-titanate	1455
Lu	1630	Hbn	27.4 [6]	1659	Hbn	1597
Hf	1720	HfO_2	1 (pure)	1684	HfO_2	1652
Ta	1546	Prv	1 (assumed ideal)	1573	Hbn + Ca-titanate	~1550
W	1736	W-Re alloy	1 (assumed ideal)	1789	Refractory metal alloy	1802
Re	1736	W-Re alloy	1 (assumed ideal)	1821	Refractory metal alloy	1819

Os	1806	Os metal	1 (pure)	1812	Refractory metal alloy	1804
Ir	1566	Os-Ir alloy	1 (assumed ideal)	1603	Refractory metal alloy	1610
Pt	1370	Fe alloy	$\ln\gamma = -59000/(8.314 \cdot T)$ [4]	1408	Refractory metal alloy	1411
Au	967	Fe alloy	$\ln\gamma = 38000/(8.314 \cdot T)$ [4]	1060	Fe alloy	1225
Hg	240	Tro	$\ln\gamma = 1000 \cdot \ln(7.4)/T$ [2]	252	Tro	
Tl	365	Tl_2S, Tl	1 (pure)	532	Tro	428*
Pb	495	PbS	1 (pure)	727	Fe alloy	496*
Bi	480	Bi metal	1 (pure)	746	Fe alloy	451
Th	1630	Hbn	1 (assumed ideal)	1659	Hbn	1545
U	1609	Hbn	1 (assumed ideal)	1610	Hbn	1420

En - enstatite; Fo - forsterite; Cpx - clinopyroxene; Mll - melilite; Pl - plagioclase; Fsp - feldspar; Ap - apatite; Crn - corundum; Hbn - hibonite; Scb - schreibersite; Tro - troilite; Sdl-sodalite; Prv - perovskite; Syl - sylvite; Sa - sanidine; $*10^{-5}$ bar

[1] Frei et al (2009); [2] This study based on lattice strain Model; [3] Orville (1972); [4] Boom et al. (1983); [5] Grimsey (1977); [6] Davis et al. (2018); [7] Arita et al. (1981); [8] Fleet (1975); [9] Predel and Vogelbein (1975); [10] Predel and Vogelbein (1979); [11] Hari Kumar et al. (1996); [12] Pei et al. (1995)

Supplementary Table 1: Thermodynamic data sources for major gases and solids considered at conditions of 50% condensation of the elements of interest from a solar gas at 10^{-4} bar. Additional solids and gases considered were those included by Wood and Hashimoto (1993) in the PHEQ database.

Element	Gaseous species	Solid phases
H	H_2, H_2O, H, HO_2, HCO, H_2CO, H_2O_2, H_2S, HCl, HF [1]	
He	-	
Li	Li, LiCl [4]	Li_2SiO_3, Li_4SiO_4 [4]
Be	Be, BeCl, $BeCl_2$, BeOH, $Be(OH)_2$ [4]	BeO [4]
B	B, BCl, BOCl, B_2O_3, BCl, BCl_2, BCl_3 [4]	B_2O_3 [4]
C	C, CH, CH_2, CH_3, CH_4, CO, CO_2, C_2H, C_2H_2, C_2O, CS, CS_2 [1]	
N	NS, N_2, NH, NH_2, NH_3 [4]	
O	O, O_2, OH, OAlH, OAlOH [1]	
F	SiF, CaF, ClF, F, F_2, HF [4]	CaF2 [4]; Ca5P3O12F [24] [15]*
Ne	-	
Na	Na, NaC, NaO, Na_2, NaH, NaOH [1]	NaCl [4]; Na4Al3Si3O12Cl [23] [11]; NaAlSi3O8 [4]
Mg	Mg, MgO, Mg_2, $Mg(OH)_2$, MgH, MgOH, MgS [1]	Mg_2SiO_4, $Mg_2Si_2O_6$, $MgAl_2O_4$ [1]
Al	Al, Al_2O, Al_2O_2, AlH, AlOH, AlO, AlO_2, Al_2, AlC, AlS [1]; Al_2O_3, $Al(OH)_2$ [2]; $Al(OH)_3$ [3]	Al2O3 [1]; CaAl12O19 [18]
Si	SiO, Si, SiO_2, SiH_4, SiH, SiS, Si_2 [1]; $Si(OH)_4$ [3]	Si, SiO_2 (Crs), SiO_2 (Qz) [1]
P	PH, PN, PH3 [5]; PS [6]; P, P2, P4, PO [4]	Ni3P [4]; Fe3P [10]; Ca5P3O12OH [9] [15]*; Ca5P3O12F [24] [15]*
S	S, SiS, S_2, SH, SO, S_2O, SO_2, SO_3 [1]	FeS, Fe0.875S [20], NiS [4]
Cl	SiCl, CaCl, NiCl, KCl, NaCl, HCl, Cl, Cl_2, Cl_2O [4]	Na4Al3Si3O12Cl [23] [11]; NaCl, KCl [4]; Ca5P3O12Cl [11] [13]
Ar	-	
K	K, KCl [4]	KCl, KAlSi3O8 [4]; KMg3AlSi3O10(OH)2 [21]
Ca	Ca, CaOH, $Ca(OH)_2$, CaO, CaS, Ca_2 [1]	CaAl2Si2O6, CaMgSi2O6, Ca2Al2SiO7, Ca2MgSi2O7 [15]; CaFeSi2O6 [19]
Sc	Sc [4]; ScO [8]	Sc_2O_3 [4]
Ti	Ti, TiO [4]	Ti, Ti_2O_3, TiO_2, $CaTiO_3$ [4]
V	V, VO, VO_2 [4]	V, V_2O_3 [4]
Cr	Cr [4]; CrO [8]	Cr, $MgCr_2O_4$, $FeCr_2O_4$ [4]
Mn	Mn [4]; MnO [8]	Mn, Mn_2SiO_3, $MnSiO_3$ [4]
Fe	Fe, $Fe(OH)_2$, FeO, FeS [1]	Fe2SiO4 [15]; Fe [1]; FeCr2O4 [4]; Fe3P [10]; FeAl2O, FeSiO3 [19]
Co	Co, CoCl [4]	Co [4]
Ni	Ni, NiCl [4]	Ni, NiS, Ni_3P, Ni_2SiO_4 [4]
Cu	Cu, CuCl, CuS, CuO [4]	Cu [4]
Zn	Zn, ZnS, $ZnCl_2$ [4]	Zn, $ZnSiO_3$, Zn_2SiO_4, ZnS [4]
Ga	Ga, GaCl, GaF, GaO [4]; GaOH [12]	Ga, Ga_2O_3 [4]
Ge	Ge, GeO, GeS [4]	Ge [4]
As	As, AsS, As_2 [4]	As [4]
Se	Se, Se_2, H_2Se [4]	$FeSe_{0.96}$ [4]
Br	Br, Br_2, HBr, KBr, NaBr [4]	NaBr, KBr [4]; Ca5P3O12Br [9]
Kr	-	
Rb	Rb, RbCl [4]	Rb_2O [4]**

Sr	Sr [4]; SrO [8]; SrS [1]	SrO, $SrTiO_3$ [4]
Y	Y [4]; YO [8]	Y_2O_3 [4]
Zr	Zr, ZrO, ZrO_2 [4]	ZrO_2 [4]
Nb	Nb [4], NbO [8]	NbO, NbO_2, Nb_2O_5 [4]
Mo	Mo, MoO, MoO_2 [4]	Mo, MoO_2 [4]
Ru	Ru [4]	Ru [4]
Rh	Rh [4]	Rh [4]
Pd	Pd [4]	Pd [4]
Ag	Ag, AgCl [4]	Ag, Ag_2S [4]
Cd	Cd, CdO, CdS [4]	CdS, $CdSiO_3$ [4]
In	In, InS, InCl [4]; InOH [16]	In, InS, In_2S_3 [4]
Sn	Sn, SnS,SnCl [4]	Sn, SnS [4]
Sb	Sb, Sb2, Sb4, SbCl, SbO [4]; SbS [14]	Sb [4]; Sb2S3 [15][4]*
Te	Te, Te_2, H_2Te [4]	$FeTe_{0.9}$ [4]
I	I, I_2, HI [4]	NaI, KI [4]
Xe	-	
Cs	Cs, CsCl [4]	Cs_2O [4]**
Ba	Ba [4]; BaO [8]; BaS [1]	$BaTiO_3$ [4]
La	La [4]; LaO [7]	La_2O_3 [4]
Ce	Ce [4]; CeO, CeO2 [7]	Ce_2O_3, CeO_2 [4]
Pr	Pr [4]; PrO [7]	Pr_2O_3 [4]
Nd	Nd [4]; NdO [7]	Nd_2O_3 [4]
Sm	Sm [4], SmO [7]	Sm_2O_3 [4]
Eu	Eu [4]; EuO [7]	EuO [7]; Eu2O3 [4]
Gd	Gd [4]; GdO [7]	Gd_2O_3 [4]
Tb	Tb [4]; TbO [7]	Tb_2O_3 [4]
Dy	Dy [4]; DyO [7]	Dy_2O_3 [4]
Ho	Ho [4]; HoO [7]	Ho2O3 [7]
Er	Er [4]; ErO [7]	Er_2O_3 [4]
Tm	Tm [4]; TmO [7]	Tm_2O_3 [4]
Yb	Yb [4]; YbO [7]	Yb_2O_3 [4]
Lu	Lu [4]; LuO [7]	Lu_2O_3 [4]
Hf	Hf [4]; HfO [8]	HfO_2 [4]
Ta	Ta, TaO, TaO_2 [4]	Ta_2O_5 [4]
W	W, WO, WO_2 [4]	W [4]
Re	Re [4]	Re [4]
Os	Os [4]	Os [4]
Ir	Ir [4]	Ir [4]
Pt	Pt [4]	Pt [4]
Au	Au, AuS [4]	Au [4]
Hg	Hg, HgS [17]	HgS [17]***
Tl	Tl, TlCl [4]; Tl2S [22]	Tl, Tl_2S [4]
Pb	Pb, PbS [4]	Pb, PbS [4]
Bi	Bi, Bi_2 [4]	Bi, Bi_2S_3 [4]
Th	Th [4]; ThO, ThO2 [7]	ThO_2 [4]
U	U [4]; UO, UO2 [7]	UO_2 [4]

* Enthalpy from first reference. Heat capacity and entropy from second.

** Feldspar modelled on Sanidine and G differences between metal oxide and K_2O

***By 1/T extrapolation of Knudsen-cell mass spectrometric measurements

[1] JANAF, Chase et al. (1985); [2] Glushko et al (1978); [3] Hashimoto (1992); [4] Barin et al. (1989); [5] Lodders (1999); [6] Lodders (2004); [7] Konings et al. (2014); [8] Pedley and Marshall (1983); [9] Cruz et al. (2005); [10] Zaitsev et al. (1995); [11] This work - see text; [12] Battat et al. (1974); [13] Drouet (2015); [14] Hino et al. (1986); [15] Robie et al. (1978); [16] Skulan et al. (2006); [17] Ferro et al. (1989); [18] Kumar and Kay (1985); [19] Wood and Hashimoto (1993); [20] Grønvold and Stølen (1992); [21] Mel'chakova et al. (2004); [22] Knacke et al. (1991); [23] Komada et al. (1995); [24] Hovis and Harlov (2010)

Figure 1

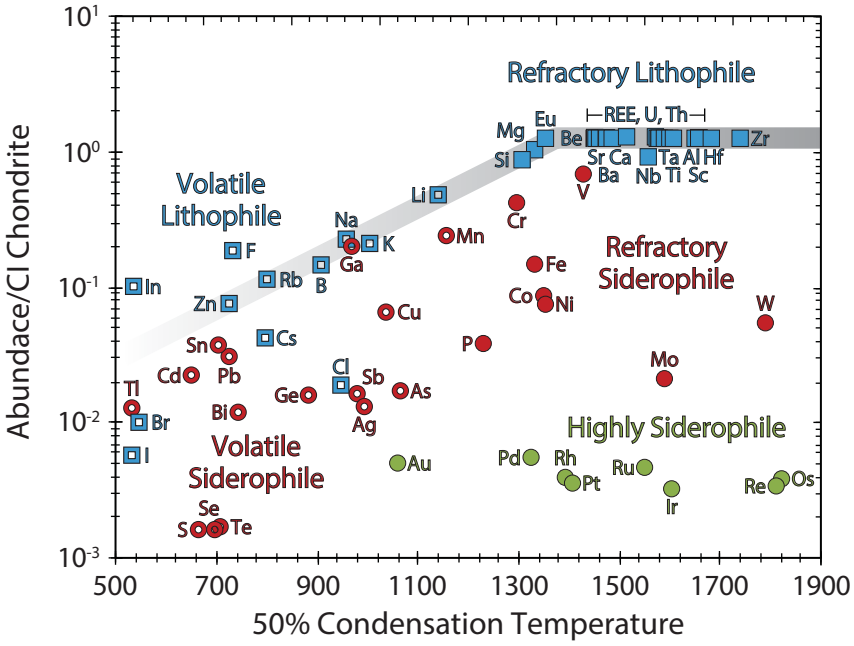
Refractory Lithophile
Volatile Lithophile
Refractory Siderophile
Highly Siderophile
Volatile Siderophile
REE, U, Th
Mg
Eu
Be
Zr
Si
Sr
Ca
Ta
Al
Hf
Ba
Nb
Ti
Sc
V
Li
Cr
Na
K
Mn
F
Ga
Fe
In
Rb
B
Co
Ni
W
Zn
Cu
Cs
P
Sn
Mo
Cd
Pb
Cl
Sb
As
Tl
Ge
Br
Bi
Ag
I
Au
Pd
Rh
Ru
Pt
Ir
Re
Os
Se
S
Te
Abundace/CI Chondrite
50% Condensation Temperature
10^{1}
10^{0}
10^{-1}
10^{-2}
10^{-3}
500
700
900
1100
1300
1500
1700
1900

Figure 2a,b

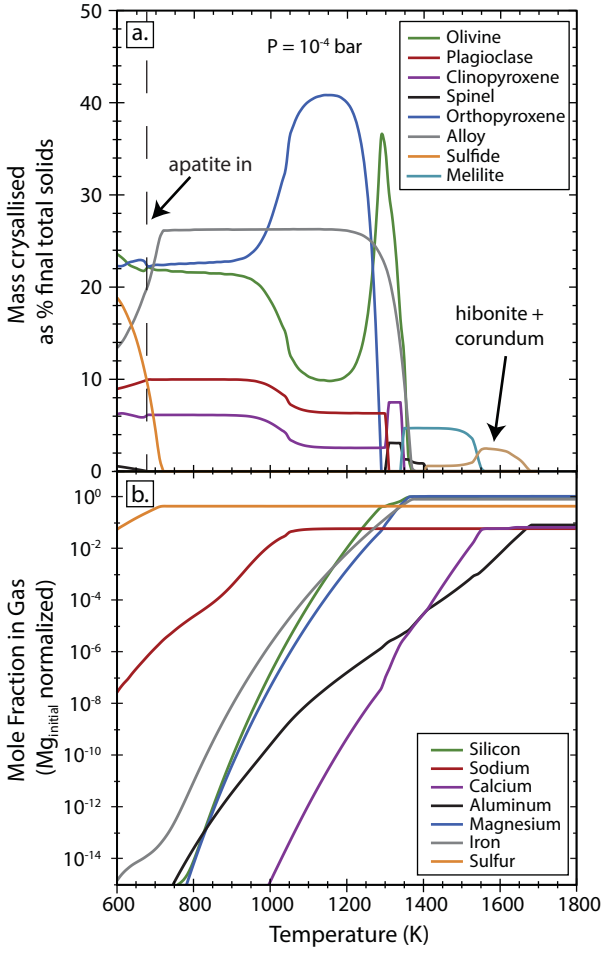
a.
P = 10⁻⁴ bar
Olivine
Plagioclase
Clinopyroxene
Spinel
Orthopyroxene
Alloy
Sulfide
Melilite
apatite in
hibonite +
corundum
Mass crysallised
as % final total solids
0
10
20
30
40
50
b.
Silicon
Sodium
Calcium
Aluminum
Magnesium
Iron
Sulfur
Mole Fraction in Gas
(Mg_initial normalized)
10⁰
10⁻²
10⁻⁴
10⁻⁶
10⁻⁸
10⁻¹⁰
10⁻¹²
10⁻¹⁴
600
800
1000
1200
1400
1600
1800
Temperature (K)

Figure 3

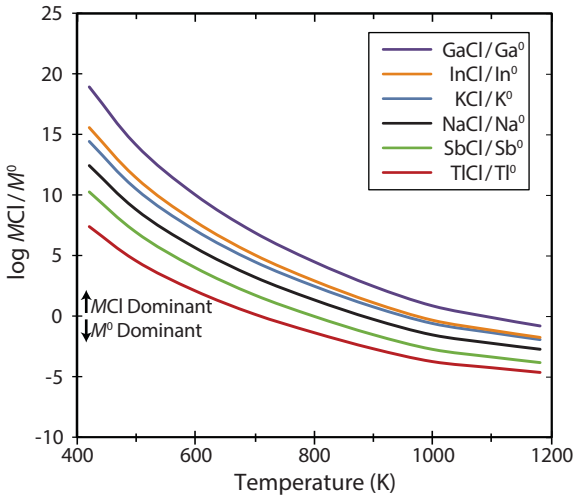
25
20
15
10
5
0
-5
-10
400
600
800
1000
1200
Temperature (K)
log MCl / M⁰
GaCl / Ga⁰
InCl / In⁰
KCl / K⁰
NaCl / Na⁰
SbCl / Sb⁰
TlCl / Tl⁰
MCl Dominant
M⁰ Dominant

Figure 4

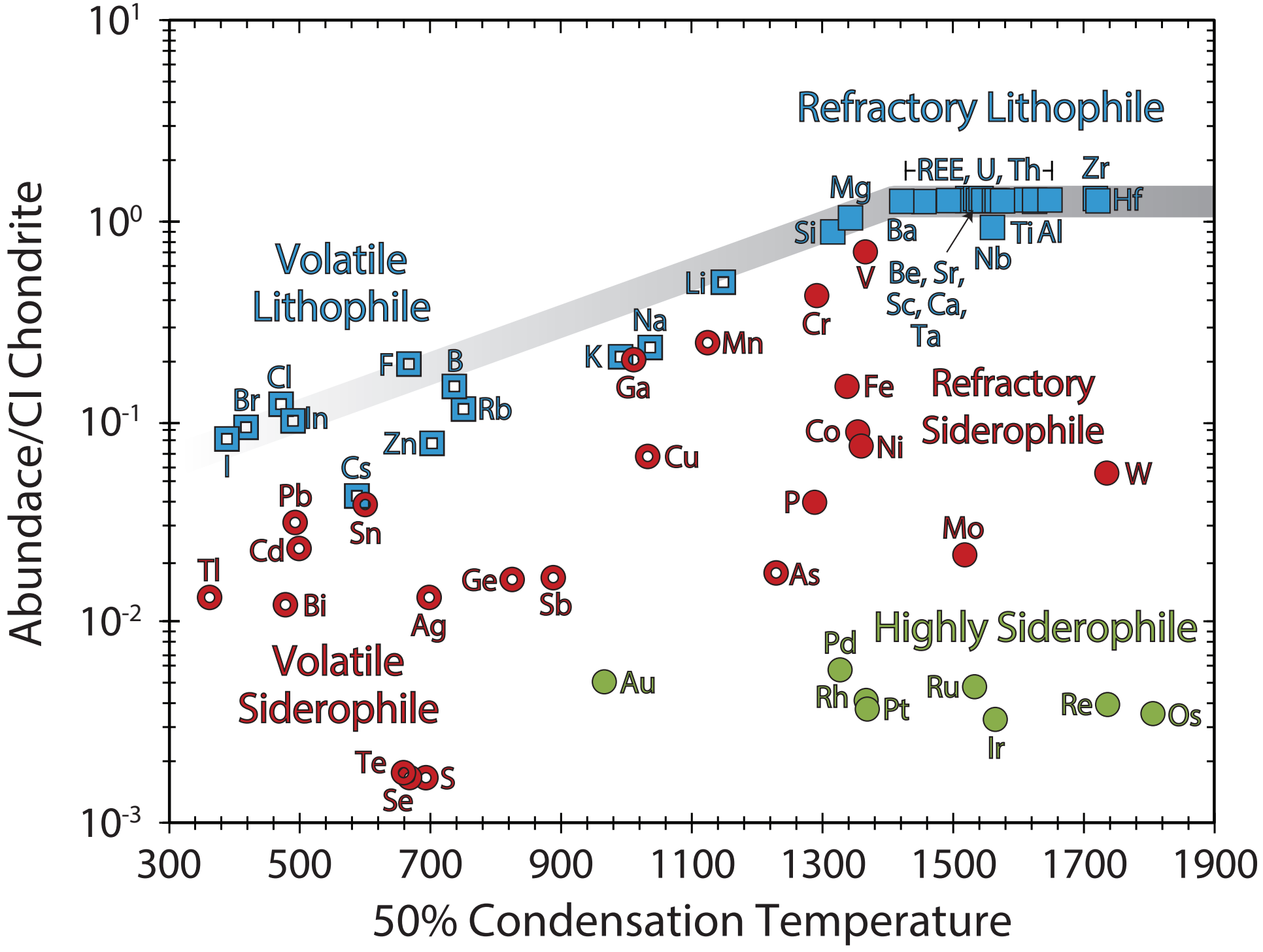
Abundace/CI Chondrite
50% Condensation Temperature
Refractory Lithophile
Volatile Lithophile
Refractory Siderophile
Volatile Siderophile
Highly Siderophile
REE, U, Th
Zr
Hf
Mg
Si
Ba
Ti
Al
Nb
V
Be, Sr, Sc, Ca, Ta
Cr
Li
Na
K
Mn
Ga
F
B
Rb
Cl
Br
In
I
Zn
Cu
Fe
Co
Ni
W
P
Mo
As
Cs
Pb
Sn
Cd
Tl
Bi
Ge
Sb
Ag
Au
Pd
Rh
Pt
Ru
Ir
Re
Os
Te
Se
S

Figure 5a,b

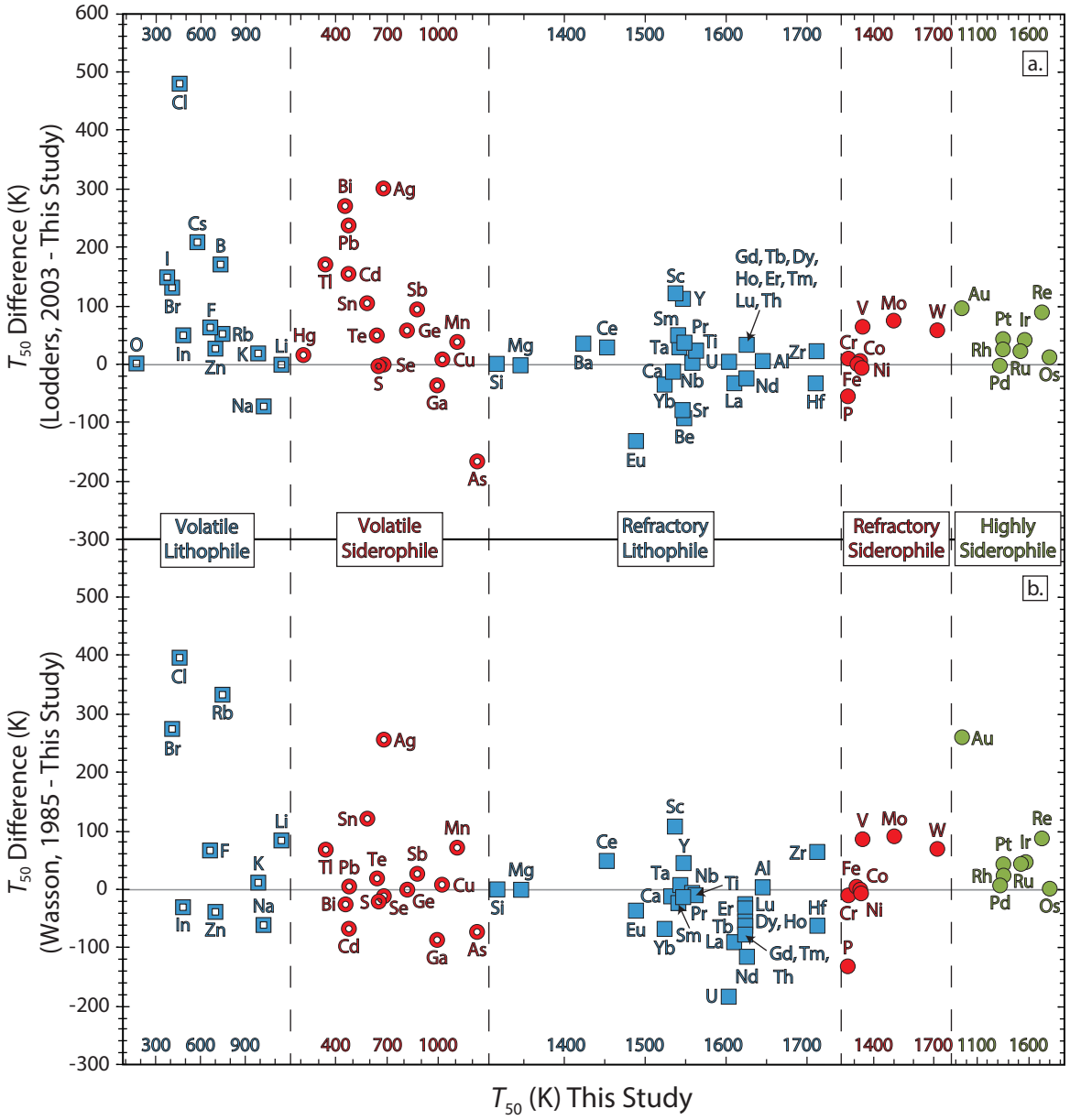
a.
b.
T_{50} Difference (K)
(Lodders, 2003 - This Study)
T_{50} Difference (K)
(Wasson, 1985 - This Study)
T_{50} (K) This Study
Volatile Lithophile
Volatile Siderophile
Refractory Lithophile
Refractory Siderophile
Highly Siderophile
Gd, Tb, Dy, Ho, Er, Tm, Lu, Th
Gd, Tm, Th
Dy, Ho